

High-velocity feature as the indicator of the stellar population of Type Ia supernovae

Xiang-Cun Meng^{1,2,3}

¹ *Yunnan Observatories, Chinese Academy of Sciences, 650216 Kunming, PR China*

² *Key Laboratory for the Structure and Evolution of Celestial Objects, Chinese Academy of Sciences, 650216 Kunming, PR China*

³ *Center for Astronomical Mega-Science, Chinese Academy of Sciences, 20A Datun Road, Chaoyang District, Beijing, 100012, P. R. China*

xiangcunmeng@ynao.ac.cn

ABSTRACT

Although type Ia supernovae (SNe Ia) are very useful in many astrophysical fields, their exact nature is still unclear, e.g. the progenitor and explosion models. The high-velocity features (HVF) in optical spectra of SNe Ia could provide some meaningful information to constrain the nature of SNe Ia. Here, I show strong evidence that the SNe Ia with strong CaII infrared triple (CaII IR3) HVF around maximum brightness associate with relatively younger population than those with weak CaII IR3 HVF, e.g. the SNe Ia with strong CaII IR3 HVF tend to occur in late-type galaxy, or early-type galaxy with significant star formation. In addition, using pixel statistics I find that the SNe Ia with strong maximum-light CaII IR3 HVF show a higher degree of association with star formation index, e.g. H α or near-UV emission, than those with weak CaII IR3 HVF. Moreover, I find that the strength of the CaII IR3 HVF is linearly dependent on the difference of the absorption-weighted velocities between CaII IR3 and SiII 635.5 nm absorption lines, which then is a good index to diagnose whether or not there is a high-velocity component in the CaII IR3 absorption feature in the spectra of SNe Ia. I finally discussed the origin of the HVFs and the constraints from our discoveries on the progenitor model of SNe Ia.

Subject headings: stars: supernovae: general - white dwarfs - circumstellar matter

1. INTRODUCTION

As the best distance indicator, the observation of Type Ia supernovae (SNe Ia) leads to the discovery of an accelerating-expansion Universe, which implies that there is a mysterious dark energy in the Universe and the evolution of the Universe is dominated by the dark energy (Riess et al. 1998; Perlmutter et al. 1999). Now, SNe Ia are becoming the center of a kind of scientific industry, such as measuring the equation of dark energy (Sullivan et al. 2011; Meng et al. 2015; Abbott et al. 2019), and constraining the cosmological model and basic physics via comparing the Hubble constant value from SNe Ia with the one from Planck satellite (Riess et al. 2016;

Planck Collaboration et al. 2018). The cosmological utility of SNe Ia as distance indicators is dependent on one property of SNe Ia, i.e. their luminosity may be standardized by the shape of their light curves (Phillips 1993; Riess et al. 1996; Perlmutter et al. 1997).

Although SNe Ia are so important for cosmology and basic physics, the exact nature of SNe Ia is still unclear. Generally speaking, SNe Ia arise from the thermonuclear explosion of carbon-oxygen white dwarfs (CO WDs) in binary systems (Hoyle & Fowler 1960), but we still do not have an exact understanding on the explosion physics and the evolution of the WDs towards explosion, i.e. various explosion and progenitor models are proposed, but no any model may explain all the prop-

erties of SNe Ia (Hillebrandt & Niemeyer 2000; Goobar & Leibundgut 2011; Wang & Han 2012; Hillebrandt et al. 2013; Maoz, Mannucci & Nelemans 2014). Spectral features may provide clues for diagnosing the explosion and progenitor models of SNe Ia (Jha et al. 2019), e.g. a variable or blueshift sodium line in early spectra indicates that at least a part of SNe Ia may originate in the single-degenerate systems (Patat et al. 2007; Sternberg et al. 2011), and a signature of the global asymmetry in the innermost ejecta from later spectra implies an off-center ignition in exploding WD (Maeda et al. 2010; Maguire et al. 2018).

Detailed spectroscopic analysis usually focuses on the absorption features of silicon with minima which may indicate typical photospheric velocities [the so-called ‘photospheric-velocity feature’ (PVF)], and be proposed as a diagnostic tool to inspect the subclasses of SNe Ia (Benetti et al. 2005; Branch et al. 2009; Wang et al. 2009). Another interesting feature in early SN Ia spectra is the ‘high-velocity feature (HVF)’, whose velocity is higher than normal PVF by 6000 - 13000 km s⁻¹ (Mazzali et al. 2005a; Maguire et al. 2014; Childress et al. 2014; Zhang et al. 2016). Since the first suggestion of HVF was made by Hatano et al. (1999), it is found that almost all SNe Ia show HVF in their early spectra (Mazzali et al. 2005b). The HVFs of SNe Ia are often seen in CaII H&K, Si II λ 6355 and CaII infrared triplet features (hereafter CaII IR3), and appear strong in their early spectra, and become weak with time (Parrent et al. 2012; Marion et al. 2013; Childress et al. 2014; Zhao et al. 2015). In addition, numerous spectropolarimetric observations show that the line-forming region for the HVFs is physically distinct from that for PVFs, and is substantially asymmetric (Wang et al. 2006; Wang & Wheeler 2008; Patat et al. 2009; Maund et al. 2013).

HVFs in SNe Ia have obtained an increasing attention and some recent studies have found some correlations between different observable quantities. For example, the strength of the HVFs was discovered to correlate with the light-curve width of SNe Ia, i.e. the SNe Ia with strong HVFs tend to have a wide light curve, while the SNe Ia with narrowest light curve favor a weak HVF (Maguire et al. 2012, 2014; Childress et al.

2014). However, although there is a clue that CaII H&K velocity correlates with host galaxy stellar mass (Maguire et al. 2012), the strength of HVFs from a larger sample seems not to be affected by the global parameters of their host galaxies (Zhao et al. 2015).

Whatever, the physical origin of the HVFs and how the features are correlated with the progenitor and explosion models of SNe Ia are still lacking. Interaction with circumstellar material (CSM) was a hot-discussing cause of the HVFs, where the CSM could be a clumpy cloud, a torus or a shell (Kasen et al. 2003; Wang et al. 2003; Patat et al. 2009; Mulligan & Wheeler 2017). In addition, the HVFs in SNe Ia may also be naturally explained by the explosion mechanism itself, e.g. gravitational confined detonation on the surface of a CO WD or the helium detonation in a CO WD envelope (Plewa et al. 2004; Kasen & Plewa 2005; Shen & Moore 2014). No matter what the origin of the HVFs, at least one of the abundance enhancement, density enhancement or ionization effect at high velocity region must be present (see the detailed discussion in Mazzali et al. 2005a)

However, although the sample of SNe Ia on the HVFs becomes larger and larger, no determinative constraint on the progenitor and explosion models of SNe Ia is obtained by studying the HVFs. Especially, why wasn’t the correlation between the strength of the HVFs and the population of SNe Ia discovered since the strength correlates with the width of the light curve (the width is an index to represent the brightness of an SN Ia, Phillips 1993; Riess et al. 1996; Perlmutter et al. 1997), while it has long been established that bright SNe Ia favor young stellar population and dim ones tend to belong to old stellar population (Hamuy et al. 1996; Wang et al. 1997; Howell 2001; Sullivan et al. 2006). In this paper, I will show strong evidence that the SNe Ia with strong HVFs belong to relatively young population, while those with weak HVFs favor relatively old population.

In Sect. 2, I describe some definitions and the data origin used in this paper. I will present my results in Sect. 3, and discuss the origin of the HVFs and the constraints of my discoveries on the progenitor models of SNe Ia in Sect. 4. In Sect. 5, I will summarize **my** main conclusions.

2. DATA

All the data used in this paper have been published in literatures or may be easily obtained from NASA/IPAC Extragalactic Database (NED). The majority of the SNe Ia used here are from Berkeley SN Ia Program (BSNIP) and have been published in Silverman et al. (2012b). In this paper, I will mainly discuss whether or not the strength of a HVF correlates with other observable quantities. If there is a high-velocity component in an absorption feature, the absorption feature may be fitted by two Gaussian profiles, i.e. one is the HVF and the other is the PVF. Following the definition in Childress et al. (2014), the strength of the HVF may be described by the ratio of the pseudo-equivalent width (pEW) of HVF absorption component to PVF absorption component, i.e.

$$R_{\text{HVF}} = \frac{\text{pEW}(\text{HVF})}{\text{pEW}(\text{PVF})}. \quad (1)$$

Generally, the strength of the HVFs decreases with time, and around the maximum light, the HVFs for some SNe Ia become very weak, and even disappear, while the other SNe Ia still show very strong HVFs. So, I choose the R_{HVF} value around the maximum light as the indicator of the strength of HVF for one SN Ia as did in Childress et al. (2014). CaII IR3 absorption line in the spectra of an SN Ia usually shows the most remarkable HVF and is widely studied. Therefore, I only focus on the CaII IR3 line, and the R_{HVF} values of CaII IR3 lines for different SNe Ia are from Silverman et al. (2015) and Zhao et al. (2015).

Meng et al. (2017) found that all SNe Ia may follow a universal polarization sequence, i.e. the polarization of SiII 635.5 nm absorption feature increases with a relative equivalent width (REW), where the REW is defined as the ratio of the pEW to the relative depth (a) of an absorption feature, i.e.

$$\text{REW} = \frac{\text{pEW}}{a}. \quad (2)$$

Meng et al. (2017) suggested that the REW of SiII 635.5 nm absorption line could be an indicator to diagnose the explosion model of SNe Ia since the REW reflects the distribution of an element in supernova ejecta. They found that the distribution of the REW of SiII 635.5 nm around maximum light may be well fitted by a Gaussian with

an average value of 157.9 Å, and then they suggested that their discovery could mean that all SNe Ia share the same explosion mechanism, and only the delayed detonation model has a potential ability to explain their discovery at present. Here, following Meng et al. (2017), I will check whether or not there is a correlation between the REW of SiII 635.5 nm absorption line and the strength of the HVF of CaII IR3 line around maximum light, where the values of pEW and a for different SNe Ia are mainly from Silverman et al. (2012a).

Childress et al. (2014) defined an average absorption-weighted velocity and found that the difference of absorption-weighted velocity between CaII IR3 and SiII 635.5 nm lines correlates with the decline rate $[\Delta m_{15}(B)]$ of the light curve of SNe Ia, where the absorption-weighted velocity is defined as

$$\bar{v} = \frac{\int v \times a(v)dv}{\int a(v)dv}, \quad (3)$$

where $a(v)$ is the normalized absorption profile in velocity space. Childress et al. (2014) presented the absorption-weighted velocities of the SiII 635.5 nm, CaII IR3, and CaII H&K lines around maximum light for 58 SNe Ia, and I will study whether or not the absorption-weighted velocities correlates with other properties of SNe Ia.

In this paper, I also want to check whether or not the strength of the CaII IR3 HVF around the maximum light correlates with the stellar population or stellar environment. The stellar environment at the location of supernova explosion may reflect the information of the stellar population of SNe Ia, and can be tested by checking SN positions in their host galaxies and the global properties of the host galaxies (Wang et al. 2013; Anderson et al. 2015a). The global parameters of the SN host galaxies, e.g. the physical size and near-ultraviolet (nUV) absolute magnitude, are obtained from NED¹ and the position information of SNe Ia in their host galaxies are from Wang et al. (2013) and Anderson et al. (2015b).

Zhao et al. (2015) found that the decay rate of R_{HVF} measured at 7 days before maximum brightness roughly correlates with $\Delta m_{15}(B)$ and $V_{\text{max}}^{\text{Si}}$ (the maximum-light photospheric velocity measured from SiII 635.5 nm absorption line). Here, I also want to check whether or not the decay rate

¹<http://ned.ipac.caltech.edu/>

of the R_{HVF} of CaII IR3 line around maximum light correlates with the host galaxy morphology, the REW value of SiII 635.5 nm absorption line and the strength of the CaII IR3 HVF around maximum light, where the decay rate of the R_{HVF} around maximum light is calculated by

$$\dot{R}_{\text{HVF}} = \frac{\Delta R_{\text{HVF}}}{\Delta t}, \quad (4)$$

where ΔR_{HVF} is the difference of the R_{HVF} value of CaII IR3 line in two spectra between before and after maximum light. Here, I only chose the SNe Ia whose CaII IR3 R_{HVF} must have a value larger than 0 before maximum light, and the spectrum phases must be within 5 days around maximum brightness. The R_{HVF} values of CaII IR3 lines for different SNe Ia are from Silverman et al. (2015).

3. RESULT

3.1. The distribution of R_{HVF} for CaII IR3 line

Silverman et al. (2015) provided a very big sample of SNe Ia from BSNIP, and 132 SNe Ia have a spectra with CaII IR3 absorption feature around maximum light (within 5 day of B-band maximum brightness). In their Table A4, the strength of the HVF of CaII IR3 absorption line for the sample are presented, as defined in Eq. (1). In Fig. 1, I show the distribution of the strength of the CaII IR3 HVF (R_{HVF}) around maximum light², where the distribution shows a peak at low value and follows a long tail until $R_{\text{HVF}} > 2.0$, i.e the stronger the CaII IR3 HVF, the lower the frequency for an SN Ia to occur. Following the definition in Childress et al. (2014), i.e. $R_{\text{HVF}} > 0.2$ means a strong HVF, about 55% of SNe Ia still present strong HVF in CaII IR3 absorption feature around maximum brightness, and some even show very strong HVF ($R_{\text{HVF}} > 0.8$). One question then arises, i.e. what factor(s) lead(s) to the different strength of the HVF between different SNe Ia. In the following sections, I will present the possible answers for the question.

²In Silverman et al. (2015) sample, the value of R_{HVF} is set to be 0 if $R_{\text{HVF}} < 0.2$. So, I set the distribution of $R_{\text{HVF}} < 0.2$ into one big bin in Fig. 1, in which 60 SNe Ia are included..

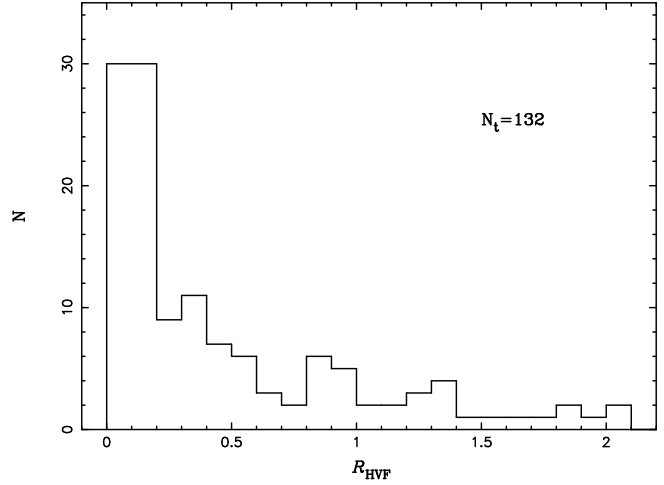


Fig. 1.— The distribution of the strength of the HVF from the CaII IR3 absorption feature around maximum light (within 5 day of B-band maximum brightness), where the data are from Silverman et al. (2015).

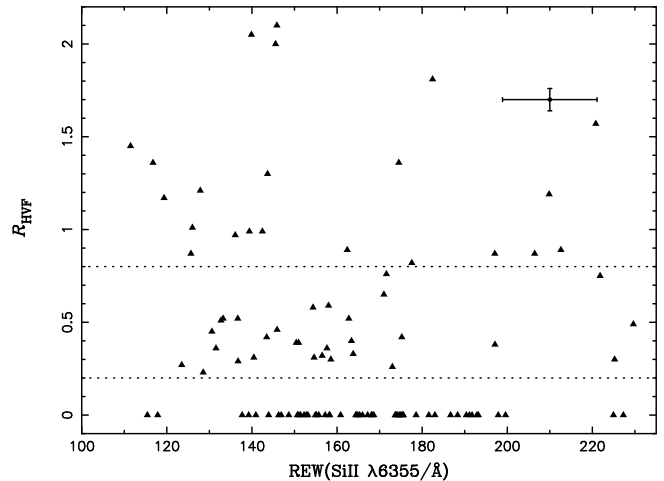


Fig. 2.— The strength of the HVF from the CaII IR3 absorption feature vs the relative equivalent width of SiII 635.5 nm line around maximum brightness, where the data are from Silverman et al. (2012a) and Silverman et al. (2015). The two dotted lines divide the sample into sub-samples with weak ($R_{\text{HVF}} < 0.2$), strong ($R_{\text{HVF}} > 0.2$) and very strong CaII IR3 HVF ($R_{\text{HVF}} > 0.8$). The black cross presents the typical error.

3.2. The relation between R_{HVF} and REW

The SiII 635.5 nm absorption line is the most remarkable feature in the optical spectra of an SN Ia around the maximum brightness and the REW of SiII 635.5 nm line could be an index reflecting the key free parameters in the delayed-detonation model (Meng et al. 2017). Fig. 2 presents the relation between the R_{HVF} of CaII IR3 absorption line and the REW of SiII 635.5 nm absorption feature around maximum light. From the first sight, there seems not to be a clear correlation between the R_{HVF} and the REW, but the SNe Ia with weak maximum-light CaII IR3 HVF mainly distribute between REW=140 and 200, while those with strong CaII IR3 HVF have a wide REW distribution. Especially, the SNe Ia with very strong CaII IR3 HVF (i.e. $R_{\text{HVF}} > 0.8$, Zhao et al. 2015) seem to disfavor the middle REW value.

In Fig. 3, I show the number distributions of the REW for the SNe Ia with weak and very strong CaII IR3 HVF around maximum light. The distributions are quite different, i.e. the SNe Ia with weak CaII IR3 HVF focus on a value of the REW between 150 and 180, while those with very strong CaII IR3 HVF are relatively rare in this region. A K-S test shows that the probability that the two sub-samples are from the same mother sample is only 1.1×10^{-3} . Meng et al. (2017) found that all kinds of SNe Ia follows a universal polarization sequence, i.e. the polarization of a SN Ia increases with the REW of SiII 635.5 nm absorption line, and then they suggested that all SNe Ia could share the same explosion model, no matter what their progenitors are. If so, the different distributions in Fig. 3 indicate that there would be another factor affecting the strength of the HVFs in SNe Ia, e.g. different progenitors (Wang et al. 2013), rather than the explosion model itself.

If I check the Branch type of the SNe Ia (Branch et al. 2009), those with a weak CaII IR3 HVF around the maximum light favor the Core normal (CN) and Cool (CL) SNe Ia, while those with a very strong CaII IR3 HVF tend to be the shallow-silicon (SS) and broad-line (BL) SNe Ia. Generally, 1991T-like SNe Ia belongs to SS group, and 1991bg-like SNe Ia belongs to CL group (Branch et al. 2009). Actually, in the sample of Silverman et al. (2015), all of the eight 1991T-like SNe Ia have a very strong

CaII IR3 HVF around the maximum light (i.e. $R_{\text{HVF}} > 0.8$), while among seventeen 1991bg-like SNe Ia, only 2002dk shows $R_{\text{HVF}} = 0.38$ and the others present weak or no CaII IR3 HVF around the maximum brightness. Such a discovery is consistent with previous results, i.e. the SNe Ia with a fast evolving light curve tend to show weak HVFs, and the SNe Ia with strong HVFs usually have a slowly evolving light curve (Maguire et al. 2012, 2014; Childress et al. 2014). It is well established that 1991T-like SNe Ia arise from relatively young stellar population and 1991bg-like SNe Ia belong to old stellar population (Howell 2001; Johansson et al. 2013a; Fisher & Jumper 2015). This result implies that the strength of the maximum-light CaII IR3 HVF could correlate with the stellar population of SNe Ia. We will address this probability in the following sections.

3.3. The relation between absorption-weighted velocities and REW

Childress et al. (2014) showed the dependence of the absorption-weighted velocities for SiII 635.5nm (\bar{v}_{Si}), CaII IR3 (\bar{v}_{CI}) and CaII H&K (\bar{v}_{CH}) features and the difference between \bar{v}_{CI} and \bar{v}_{Si} on $\Delta m_{15}(B)$ to verify that the correlation between the strength of CaII IR3 HVF and $\Delta m_{15}(B)$ are not artefact. In Figs. 4 and 5, I also show the dependence of these properties on the REW of SiII 635.5 nm absorption line around the maximum brightness. Fig. 4 shows that \bar{v}_{CI} and \bar{v}_{CH} do not significantly depend on REW, while \bar{v}_{Si} seems to slightly increase with REW, i.e. no significant physical correlation exists between the absorption-weighted velocities and the REW of SiII 635.5 nm line. However, Fig. 5 presents a clear trend that the larger the difference between \bar{v}_{CI} and \bar{v}_{Si} , the smaller the REW of SiII 635.5 nm absorption line. Especially, the SNe Ia with smaller REW (or larger difference between \bar{v}_{CI} and \bar{v}_{Si}) tend to have a stronger HVF of CaII IR3 line as indicated in Fig. 2. In addition, Fig. 5 already indicates a fact that the strength of the CaII IR3 HVF would depend on the difference between \bar{v}_{CI} and \bar{v}_{Si} .

In Fig. 6, I show the correlation between the strength of the CaII IR3 HVF and the difference between \bar{v}_{CI} and \bar{v}_{Si} around maximum brightness. There is a very good linear relation between the strength of the HVF and the veloc-

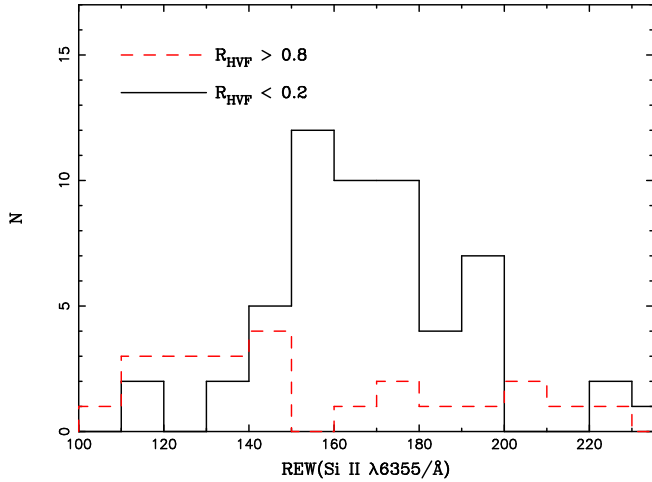


Fig. 3.— The number distributions of the relative equivalent width of SiII 635.5 nm line for SNe Ia with weak (solid line) and very strong CaII IR3 HVF (dashed line) around maximum light, respectively.

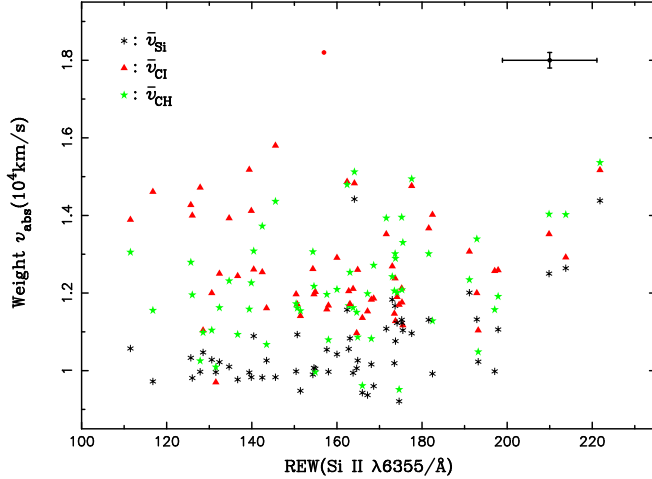


Fig. 4.— Absorption-weighted velocities for SiII 635.5nm, CaII IR3 and CaII H&K features, respectively (\bar{v}_{Si} , black asterisks; \bar{v}_{CI} , red triangles; \bar{v}_{CH} , green stars), versus the relative equivalent width of SiII 635.5 nm absorption line around the maximum light. The absorption-weighted velocity data are from Childress et al. (2014), while the relative equivalent width data are from Silverman et al. (2012a), and the cross represents the typical error of the data.

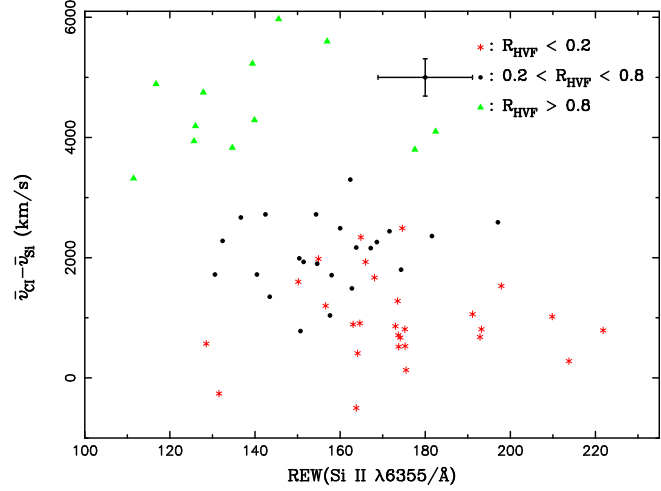


Fig. 5.— The difference between \bar{v}_{CI} and \bar{v}_{Si} versus the relative equivalent width of SiII 635.5 nm line around the maximum brightness. Different points represent the different range of CaII IR3 R_{HVF} . The absorption-weighted velocity data are from Childress et al. (2014), while the relative equivalent width data are from Silverman et al. (2012a). The cross represents the typical error of the data.

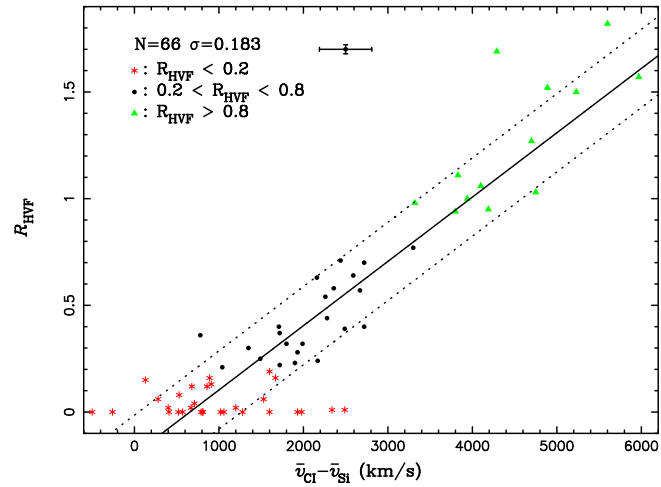


Fig. 6.— The relation between the strength of the HVF of CaII IR3 line and the difference between \bar{v}_{CI} and \bar{v}_{Si} around maximum brightness. Different points represent the different range of CaII IR3 R_{HVF} . The solid line shows a linear fit of the data and the two dotted lines present the 1σ statistic error of the fit. The data are from Childress et al. (2014), and the cross represents the typical error of the data.

ity difference, i.e. the larger the velocity difference, the stronger the CaII IR3 HVF [$R_{\text{HVF}} = -0.198 + 3.013 \times 10^{-4}(\bar{v}_{\text{CI}} - \bar{v}_{\text{Si}})$]. Such a relation is mainly from a fact that all SNe Ia have a similar absorption-weighted velocity of SiII 635.5 nm absorption line around maximum brightness, and then the strength of the CaII IR3 HVF is mainly dominated by its absorption-weighted velocity, as shown in Fig. 7, which presents the relation between the R_{HVF} of the CaII IR3 line and the absorption-weighted velocity \bar{v}_{CI} and \bar{v}_{Si} . Fig. 7 also shows a linear relation between the strength of the CaII IR3 HVF and \bar{v}_{CI} , but the scatter of the linear fit is much larger than that in Fig. 6, i.e. the difference between \bar{v}_{CI} and \bar{v}_{Si} is the indicator to measure the strength of the CaII IR3 HVF.

In addition, Fig. 6 shows that some SNe Ia with $R_{\text{HVF}} = 0$ have a large value of $(\bar{v}_{\text{CI}} - \bar{v}_{\text{Si}})$, even larger than 2000 km s^{-1} . Based on the linear relation found Fig. 6, these SNe Ia would show $R_{\text{HVF}} \sim 0.2 - 0.5$. Similarly, some SNe Ia without CaII HVF also significantly deviate from the linear fit in Fig. 7. Maybe, these SNe Ia also have a line-forming region for HVFs in the supernova ejecta, but the region overlaps with or does not distinct from the one for PVFs, which could be the reason why these SNe Ia show a significantly larger photospheric pEW value than other SNe Ia with weak CaII IR3 HVF, e.g. SN 2000dk, 2006X, 2006gt, 2007ba and 2007fr (see Table 2 in Childress et al. 2014). A piece of evidence supporting such an idea is from SN 2006X. In Childress et al. (2014), the pEW of the photospheric CaII IR3 line in the maximum-light spectrum of SN 2006X is $320 \pm 1 \text{ \AA}$, without HVF, but in Silverman et al. (2015), the pEW of the photospheric CaII IR3 line in the same spectrum is $166.6 \pm 5.3 \text{ \AA}$, with very strong HVF, i.e. $R_{\text{HVF}} = 0.89 \pm 0.03$ (see also Zhao et al. 2015). Such a different result could be derived from a fact that Silverman et al. (2015) have a series of spectra on SN 2006X from a very early phase to a phase after maximum light, while Childress et al. (2014) only analyze one spectrum at $t = 2$ day. Based on the evolution of the spectra, it would be relatively easy for Silverman et al. (2015) to judge whether or not there is a high-velocity component in a CaII IR3 absorption feature, and to estimate the possible strength of the HVF. So, based on the result in Fig. 6, the difference between \bar{v}_{CI} and \bar{v}_{Si} becomes a very good indicator which may be helpful

to judge whether or not there is a CaII IR3 HVF in the spectrum of an SN Ia, i.e. if the difference is larger than 1000 km s^{-1} , it is likely that there is high-velocity component in the CaII IR3 absorption feature, even if a single Gaussian profile may fit the feature.

3.4. The distribution of R_{HVF} for HVG and LVG SNe Ia

Observationally, the photospheric velocity decreases with time, but with different temporal velocity gradient. Based on the different velocity gradient, Benetti et al. (2005) divided normal SNe Ia into two sub-groups, i.e. high-velocity gradient (HVG) and low-velocity gradient (LVG) SNe Ia. The different velocity gradient could reflect the view angle relative to an asymmetric explosion center, i.e. the LVG SNe Ia are viewed from the direction of the off-center initial sparks, while the HVG ones are viewed from the opposite direction (Maeda et al. 2010). In Fig. 8, I show the distributions of the R_{HVF} of CaII IR3 line around the maximum brightness for HVG and LVG SNe Ia, respectively. The two distributions look similar to that shown in Fig. 1, i.e. a peak at low R_{HVF} and a long tail of high R_{HVF} . Similarly, the difference of the cumulative percent distributions of the R_{HVF} between HVG and LVG SNe Ia are also not significant. A K-S test shows that the probability that the two sub-samples are from the same mother sample is as high as about 60%. Then, the strength of the HVF of CaII IR3 line around maximum brightness could not depend on the view angle to the asymmetric explosion center, if the velocity gradient reflects the view angle. This result could indicate that the HVFs in the spectra of SNe Ia could not be derived from the explosion mechanism of SNe Ia.

3.5. The dependence of R_{HVF} on the host galaxy type

Zhao et al. (2015) checked the potential dependence of the number distributions of SNe Ia with strong and weak HVFs on their host galaxy morphologies, the K-band absolute magnitude of the host galaxies and the normalized radial distance of the SNe Ia in their host galaxies, and did not find significantly dependence on these parameters. Such a result seems to suggest that there is not a correlation between the strength of HVFs

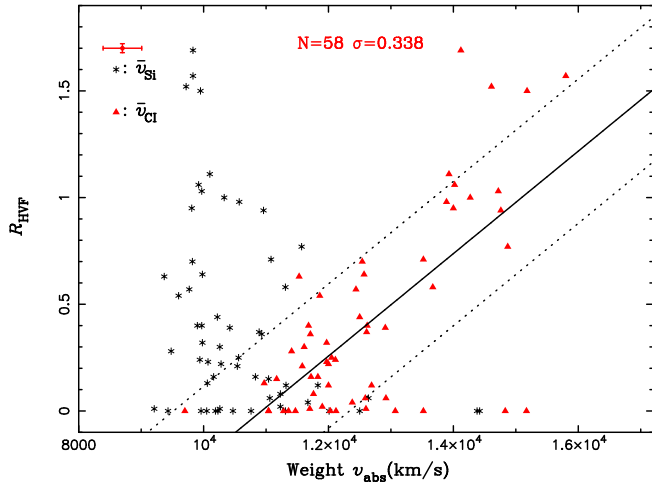


Fig. 7.— The relation between the strength of the HVF of CaII IR3 line and the absorption-weighted velocity \bar{v}_{CI} and \bar{v}_{SI} . The solid line shows a linear fit between R_{HVF} and \bar{v}_{CI} , and the two dotted lines present the 1σ statistic error of the fit. The data are from Childress et al. (2014), and the cross represents the typical error of the data.

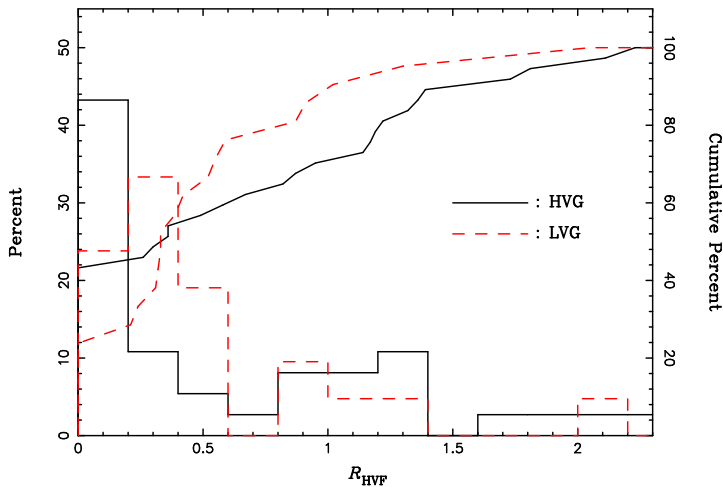


Fig. 8.— The number and cumulative percent distributions of the R_{HVF} of CaII IR3 line around maximum brightness for HVG (solid line) and LVG (dashed line) SNe Ia, respectively. The data are from Silverman et al. (2015).

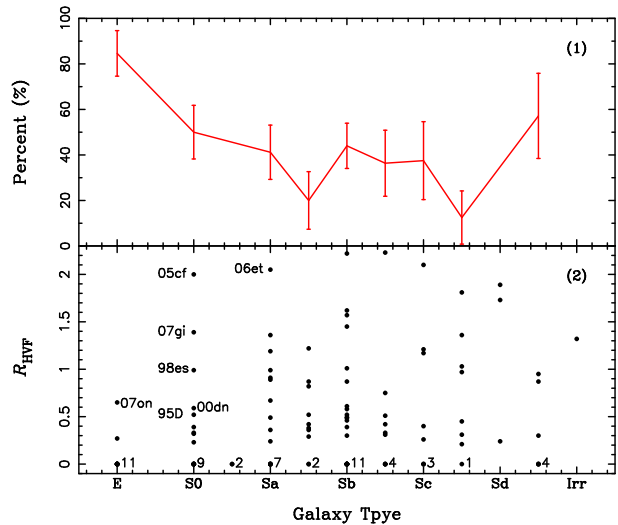


Fig. 9.— Panel (1) shows the number fraction of the SNe Ia with $R_{HVF} = 0$ as a function of host galaxy morphology, and the bars show the statistic error of the number fraction, assuming a binomial distribution (Cameron 2011). Panel (2) shows the R_{HVF} of CaII IR3 line around maximum brightness versus the galaxy morphology, where the spiral galaxies with and without a bar are not discriminated. The numbers at the bottom represent the number of SNe Ia with $R_{HVF} = 0$ in every host galaxy morphology. The R_{HVF} data are from Silverman et al. (2015), and the host galaxy morphologies are from Silverman et al. (2012b) or NED.

and the stellar population (but see Pan et al. 2015). However, the number distribution could not completely reflect the intrinsic dependence of the strength on the stellar population. Here, I want to check the potential dependence again by another way, i.e. directly studying the relation between the strength of HVFs and the parameters indicating the stellar population of SNe Ia. In Fig. 9, I show the R_{HVF} of SNe Ia and the number fraction of the SNe Ia with weak maximum-light CaII IR3 HVF ($R_{\text{HVF}} = 0$) as a function of host galaxy morphology. In the host galaxy with a morphology later than S0, the number fractions of the SNe Ia with weak maximum-light CaII IR3 HVF are not significantly different with each other within error, which is a similar result to that found in Zhao et al. (2015). However, the number fraction of the SNe Ia with weak maximum-light CaII IR3 HVF in elliptical galaxies seems to be higher than that in later type galaxies, which imply that the SNe Ia with weak CaII IR3 HVF favor old stellar population. Most of the SNe Ia with strong maximum-light CaII IR3 HVF tend to occur in later type galaxies, in which the star formation rates are generally high. Although a high star formation generally favor core-collapse SNe, arising from short-lived progenitors, it may also increase the birth rate of SNe Ia relative to the genuinely old stellar population (Della Valle & Livio 1994; Navasardyan et al. 2001). Then, the result here could indeed imply that the SNe Ia with strong HVFs belong to relatively young population.

Whatever, there are still some SNe Ia presenting a strong CaII IR3 HVF around maximum brightness in elliptical and lenticular galaxies, e.g. SN 1995D, 1998es, 2000dn, 2005cf, 2007gi and 2007on. Generally, elliptical and lenticular galaxies are passively evolving and don't contain any young stars. However, we should keep in mind that many early-type galaxies present recent star formations (Salim et al. 2005; Schawinski et al. 2007). Then, I checked the detailed circumstance of these SNe Ia. SN 2005cf has a highest maximum-light CaII IR3 R_{HVF} among SNe Ia hosted in lenticular galaxies and its host galaxy is a peculiar lenticular galaxy (MCG -01-39-003), interacting with its neighbor. There is a tidal bridge between MCG -01-39-003 and its neighbor, and SN 2005cf locates close to the tidal bridge (Pastorello et al. 2007). It is widely known that

the interaction between galaxies may enhance the star formation rate. In addition, the blue ultraviolet color of the galaxy from *Galaxy Evolution Explorer* (GALEX) also indicates a high star formation rate in MCG -01-39-003 (Smith et al. 2010). Then, SN 2005cf would associate with a relatively young population.

SN 2007gi is another one with very high maximum-light CaII IR3 R_{HVF} in a lenticular galaxy. Strictly speaking, the host galaxy of SN 2007gi (NGC 4036) is not a typical lenticular galaxy, but a morphology between S0 and Sa, with strong activity which is another index to trigger the star formation in a galaxy (Véron-Cetty & Véron 2006; Ann et al. 2015b). Interestingly, SN 2007gi just locates close to the inner activity region (Zhao et al. 2015). For SN 1998es, although the morphology of its host galaxy (NGC 0632) is classified into S0, the star formation phenomena in the galaxy are very strong and it is a star-burst galaxy (Balzano 1983). The case for SN 2007on is also very interesting, i.e. its host galaxy (NGC 1404) interacted with its neighbor galaxy (NGC 1399) about 1.2 Gyr ago and there are a large amount of intracluster medium between these two galaxy (Sheardown et al. 2018). Now, NGC 1404 is falling into the center of Fornax cluster and interacting with the intracluster medium to form a sharp leading edge, where SN 2007on just locates close to (Su et al. 2011; Gall et al. 2018). For the host galaxies of SN 1995D (NGC 2962) and 2000dn (IC 1468), there are rings/arms around their main bodies and the rings/arms are significantly bluer than their main bodies, which indicate the star formation activities or relatively young stellar population in the galaxies (Marino et al. 2011). These two NSe Ia locate either at a arm tail or close to one rings (Zhao et al. 2015, see also the image in SIMBAD³). According to above detailed check, we find that these SNe Ia with strong maximum-light CaII IR3 HVF in early type galaxies also correlate with star formation activity or relatively young stellar population (see also Pan et al. 2015). If these SNe Ia correlating with young stellar population are eliminated, the number fraction of the SNe Ia with weak maximum-light CaII IR3 HVF in lenticular galaxies would also significantly

³<http://simbad.u-strasbg.fr/simbad/sim-fbasic>

higher than that in later type galaxies, as shown in elliptical galaxies, i.e. the SNe Ia with weak maximum-light CaII IR3 HVF favor old stellar population.

3.6. The dependence of R_{HVF} on the global parameters of host galaxies

Zhao et al. (2015) checked the potential dependence of the number distribution of SNe Ia with different R_{HVF} on the K-band absolute magnitudes of host galaxy, and no significant difference between the strong and weak HVF samples is found. Here, I also want to check whether or not the R_{HVF} value depends on the other global parameters of the host galaxies, e.g. physical sizes and nUV-band absolute magnitude. In Fig. 10, I show the CaII IR3 R_{HVF} value of SNe Ia around maximum brightness as a function of the physical size (major axis) of their host galaxies, but I do not find any potential correlation between R_{HVF} and the major axis, i.e. the number distributions of the physical size of the host galaxies for the SNe Ia with weak and strong maximum-light CaII IR3 HVFs are indistinguishable.

In section 3.5, I find a clue that the CaII IR3 R_{HVF} value of SNe Ia around maximum brightness could correlate with their stellar population, but the number distribution of SNe Ia with different R_{HVF} does not rely on the K-band absolute magnitudes of their host galaxies (Zhao et al. 2015). Such an inconsistency might be derived from that the K-band absolute magnitude of a host galaxy is not a good index reflecting the star formation in the galaxy, and the K-band light in a galaxy is generally dominated by old stellar population (Mannucci et al. 2005). However, the ultraviolet absolute magnitude of a host galaxy would be a better index in the galaxy (Salim et al. 2005; Schawinski et al. 2007). I obtained the GALEX nUV absolute magnitudes of the host galaxies of SNe Ia in the sample of Zhao et al. (2015) and Silverman et al. (2015) from NED to check the potential correlation between the maximum-light CaII IR3 R_{HVF} value of SNe Ia and the nUV absolute magnitudes of their host galaxies (Fig. 11). Again, the distributions of nUV absolute magnitudes of the host galaxies of the SNe Ia with strong and weak CaII IR3 HVF are indistinguishable, i.e. a K-S test shows that the sub-samples with $R_{\text{HVF}} > 0.2$ and $R_{\text{HVF}} < 0.2$ have a proba-

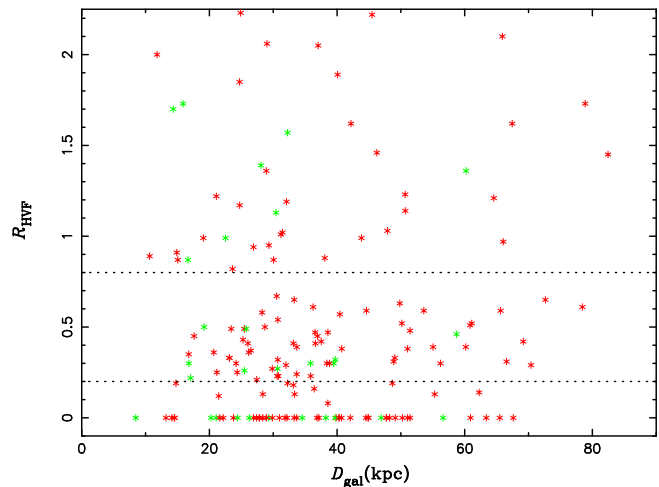


Fig. 10.— The CaII IR3 R_{HVF} around maximum brightness versus the physical sizes (major axis) of host galaxies, where the red points means that the sizes are represented by the B-band light major axis at 25 mag arcsec⁻² isophote, while the green ones by SDSS r-band major axis at 25 mag arcsec⁻² isophote. The R_{HVF} data are from Silverman et al. (2015) and Zhao et al. (2015), and the physical sizes of host galaxies are from NED. The two dotted lines divide SNe Ia into weak ($R_{\text{HVF}} < 0.2$), strong ($0.2 < R_{\text{HVF}} < 0.8$) and very strong ($R_{\text{HVF}} > 0.8$) subgroups.

bility of 46% to be from the same mother sample. However, it seems that most of SNe Ia locate in a declining zonal, as dotted lines show. The results in this section seem to be inconsistent with that discovered in section 3.5, which could be derived from the fact that the global parameters of a host galaxy is not a good tracer of stellar population at the site of supernova explosion. The global parameters of a host galaxy only represent the average information of the stellar population in the host galaxy, and could erase the intrinsic relation between SN Ia properties and their stellar populations.

3.7. Pixel statistics

The most direct method to determine the progenitor nature of an SN Ia is to investigate its pre-explosion image (Li et al. 2011; McCully et al. 2014). Such cases are rare and therefore the statistics remain low, since it is only possible for events in very nearby host galaxies. Another way is to investigate how the properties of SNe Ia vary with different global parameters of their host galaxies, as discussed in section 3.6. However, this method could erase the intrinsic relation between SN Ia properties and the information of their stellar populations, because the global parameters of a host galaxy may only represent the average information of the stellar population in the host galaxy, which could be the reason why no correlation is found between the strength of HVF and the global parameters of the host galaxies in section 3.6 and in Zhao et al. (2015). An intermediate method to constrain the nature of SN Ia progenitors is to investigate the environments at the position of an SN Ia in its host galaxy, e.g. the statistical analysis of a fractional flux or a normalized cumulative rank (NCR) pixel value function of the host galaxies at the SN explosion site (Fruchter et al. 2006; Anderson & James 2008). Generally, the core-collapse SNe approximately linearly trace the star-formation region (light) in their host galaxies, while SNe Ia do not (Anderson et al. 2015a,b). Here, I will also use this method to check whether or not there is a difference of the environments between the SNe Ia with strong and weak CaII IR3 HVF around the maximum light.

In Fig. 12, I show the cumulative distribution of the fractional flux of the host galaxies at SN explosion site for the SNe Ia with strong and weak CaII

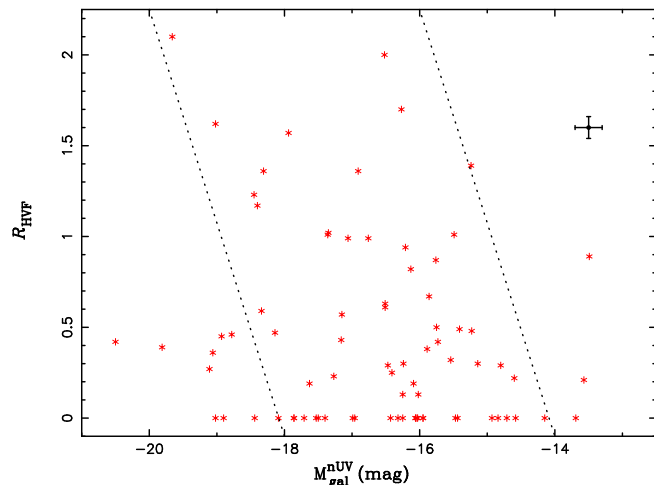


Fig. 11.— The CaII IR3 R_{HVF} around maximum brightness versus the GALEX nUV band absolute magnitudes of host galaxies. The cross shows the typical error of the data. The R_{HVF} data are from Silverman et al. (2015) and Zhao et al. (2015), and the nUV-band absolute magnitudes of host galaxies are from NED.

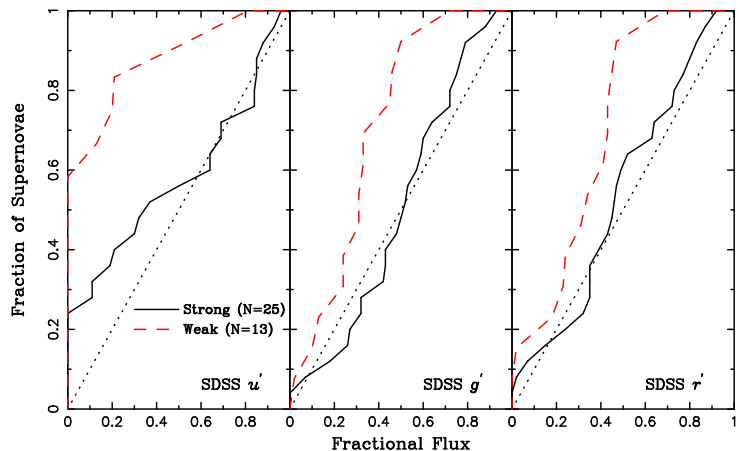


Fig. 12.— The cumulative distribution of the fractional flux of the host galaxies at the SN explosion site for SNe Ia with strong (black solid line) and weak (red dashed line) CaII IR3 HVF around the maximum light, respectively, in SDSS u' , g' and r' bands. The fractional flux data are from Wang et al. (2013).

IR3 HVF around the maximum light, respectively, in SDSS u' , g' and r' bands, where the fractional flux of an SN Ia represents the fraction of total host light in pixels fainter than or equal to the light in the pixel of SN Ia site in its host-galaxy image (Fruchter et al. 2006). A young population will trace the diagonal line in the plot, while an old population will be far away from the diagonal line. The figure shows that no matter what the SDSS band, the cumulative distribution of the SNe Ia with strong CaII IR3 HVF is closer to the line tracing the star-formation region than that of the SNe Ia with weak HVF, although the distributions for g' and r' are similar. A 2D K-S test for u' and g' bands or u' and r' bands shows that the probability that the two sub-samples are from the same mother sample is lower than 1.5%, i.e. the SNe Ia with strong maximum-light CaII IR3 HVF are more likely to be from the relatively young stellar population, while those with weak maximum-light CaII IR3 HVF tend to be from the relatively old stellar populations. Whatever, the cumulative distributions for g' and r' bands are much closer to the diagonal line than those for u' band, especially for the SNe Ia with weak CaII IR3 HVF, which indicate that g' and r' band lights would not be good tracers for the star formation in a galaxy. However, nUV and H α bands are good choices (Anderson et al. 2015a,b).

The definition of an NCR value is different from the fractional flux. The NCR value of a pixel is equal to the flux-count ratio between this pixel and the one with the highest flux count within the image of a host galaxy. Then, an NCR value is between 0 and 1, where a value of 0 means that a pixel in the image is consistent with zero flux or sky values, while a value of 1 means that the pixel has the highest flux count in the image. Whether or not the distribution of the NCR value for a given band in a cumulative plot follows a diagonal one-to-one relation may provide constraints on the population and progenitor properties of SNe Ia, i.e. a very young population will trace the diagonal one-to-one relation, while an old population will be far away from the diagonal one-to-one relation. In another words, the closer the cumulative line to the diagonal one-to-one relation, the younger the population of SNe Ia (Anderson & James 2008; Anderson et al. 2015b). Figs. 13 and 14 present the cumulative NCR dis-

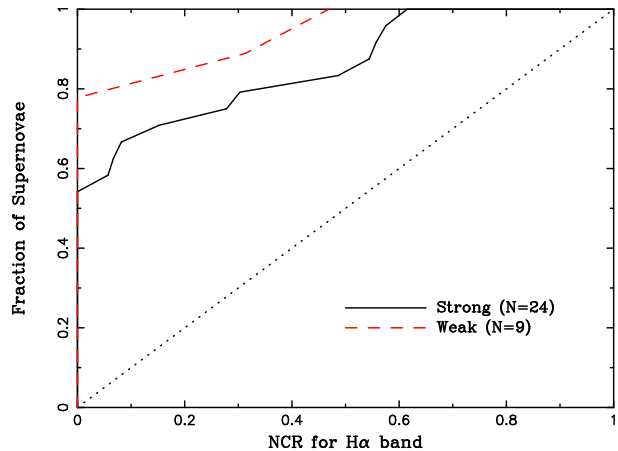


Fig. 13.— The cumulative NCR distributions of the SNe Ia with strong (black solid line) and weak (red dashed line) CaII IR3 HVF around the maximum light, respectively, for H α band. The NCR data of the host galaxies at SN Ia explosion site are from Anderson et al. (2015b).

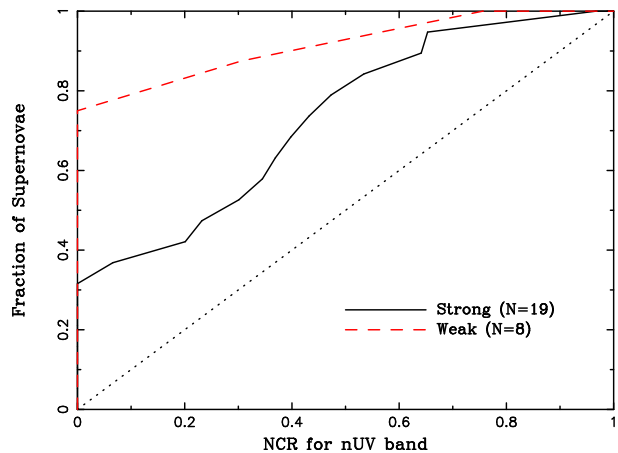


Fig. 14.— The cumulative NCR distributions of the SNe Ia with strong (black solid line) and weak (red dashed line) CaII IR3 HVF around maximum light, respectively, for nUV band. The NCR data of the host galaxies at SN Ia explosion site are from Anderson et al. (2015b).

tributions of the SNe Ia with strong and weak CaII IR3 HVF around the maximum light for H α and nUV bands, respectively. These figures show that whatever the maximum-light CaII IR3 HVF is strong or weak, or whatever the band is, the cumulative distributions of the NCRs do not trace the diagonal line, which indicates that the progenitors of SNe Ia do not belong to very young population (see also Anderson et al. 2015a,b). This also verifies that the SDSS g' and r' bands are not good tracers for star formation. However, the cumulative distribution for the SNe Ia with strong maximum-light CaII IR3 HVF is always closer to the diagonal line than the one for the SNe Ia with weak maximum-light CaII IR3 HVF, for both H α and nUV bands, which indicates that the populations of the SNe Ia with strong maximum-light CaII IR3 HVF are relatively younger than those with weak maximum-light CaII IR3 HVF. A 2D K-S test for the distributions of NCR value for H α and nUV bands between the sub-samples of the SNe Ia with strong and weak CaII IR3 HVF shows that the probability that the two sub-samples are from the same mother sample is only 2.3%, i.e. they arise from different mother sample.

3.8. Radial analysis

The delay time⁴ Comparing with the core-collapse SNe, SNe Ia have a significant delay time from star formation to explosion, and then they are very possible to explode at a position far away from their birth sites. Since a stellar population with different age and metallicity in a galaxy locates at different characteristic galactocentric radial positions, I may further investigate the environments of SNe Ia by exploring the position of SNe Ia with respect to the radial distribution of different stellar populations, e.g. a ‘Fr’ fractional flux value may provide such an information. Here, only H α band is considered (Anderson et al. 2015b). A value of Fr = 0 for an SN Ia means that the SN Ia locates at the central peak pixel in the H α band image of its host galaxy, while a value of Fr = 1 implies that the SN Ia exploded at an outer region of its host galaxy, where the

⁴The delay time is the elapsed timescale from the primordial system formation to the supernova explosion. of an SNe Ia shares the similar meaning of its stellar population to a great extent. An SN Ia with a long delay time belongs to old population, and vice versa.

H α band flux is even equal to the sky value (see details in Anderson et al. 2015b). Generally, in the cumulative plot for Fr, the cumulative fraction for a young population increases more quickly at low Fr value than an old population. In Fig. 15, we present the cumulative distribution of the Fr value for the SNe Ia with strong and weak CaII IR3 HVF around the maximum brightness, respectively. As said above, the cumulative value for the SNe Ia with strong maximum-light CaII IR3 HVF increases more quickly at low Fr value than those with weak maximum-light CaII IR3 HVF, i.e. the distributions indicate that the SNe Ia with strong maximum-light CaII IR3 HVF belong to relatively younger population than those with weak maximum-light CaII IR3 HVF. A K-S test for the distributions of Fr value shows that the probability that the two sub-samples are from the same mother sample is only 3.7%, i.e. they are from different mother samples.

Here, the sample size of the SN Ia with weak maximum-light CaII IR3 HVF is much smaller than that with strong maximum-light CaII IR3 HVF, which is probably from the fact that all the host galaxies in Anderson et al. (2015b) are star-forming galaxies. Actually, combining the small sample of the SN Ia with weak maximum-light CaII IR3 HVF, this fact is another piece of evidence to support our discovery, i.e. the SNe Ia with strong maximum-light CaII IR3 HVF are more likely to correlate with a relatively young population.

3.9. Decay rate of R_{HVF}

Above sections have shown that the SNe Ia with very strong CaII IR3 HVF around maximum light tend to occur in later type host galaxies, and some statistical analysis also show that these SNe Ia correlate with relatively younger stellar population than those with weak CaII IR3 HVF. Since I only check the dependence of the R_{HVF} values of SNe Ia at maximum brightness on their exploding environments, our results might imply that SNe Ia in relatively young environments have a slower decay rate of R_{HVF} than those in old environments. By calculating the average value of the various measurable parameters of SNe Ia, Zhao et al. (2015) found that the decay rate of the HVFs roughly correlates with $\Delta m_{15}(B)$ and $V_{\text{max}}^{\text{Si}}$. So, since it is widely known that the bright SNe Ia favor

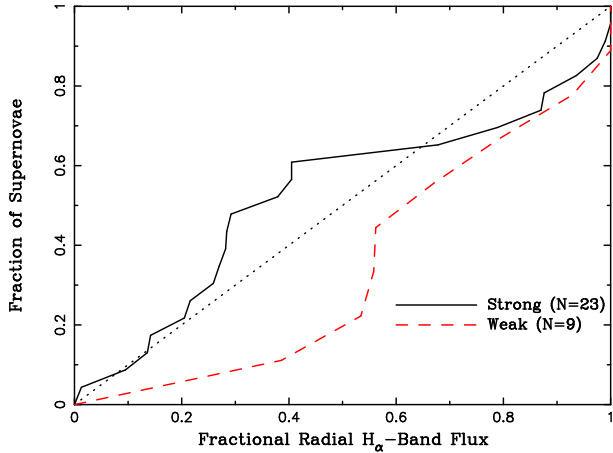


Fig. 15.— The cumulative distribution of Fr value for the SNe Ia with strong (black solid line) and weak (red dashed line) CaII IR3 HVF around maximum light, respectively. The Fr data of the host galaxies at SN Ia site are from Anderson et al. (2015b).

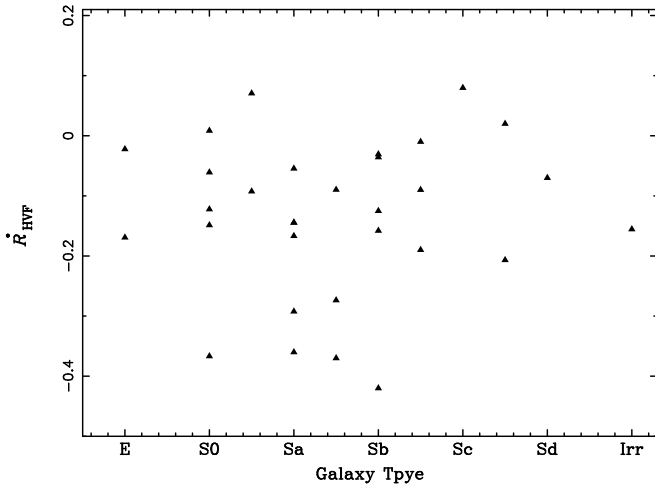


Fig. 16.— The decay rate of R_{HVF} for CaII IR3 absorption line around maximum brightness versus host galaxy morphology, where the data are from Silverman et al. (2012b) and Silverman et al. (2015).

late type galaxy (Hamuy et al. 1996; Wang et al. 1997), we would expect that the decay rate of the strength of the CaII IR3 HVF correlates with the host galaxy morphology.

In Fig. 16, I show the decay rate of R_{HVF} for CaII IR3 absorption line (\dot{R}_{HVF}) around the maximum brightness as a function of the host galaxy morphology. Here, I do not find any potential correlation between \dot{R}_{HVF} and the host galaxy morphology. The difference from that in Zhao et al. (2015) could be from that their decay rate is measured at 7 days before maximum brightness, while measured around the maximum brightness here. However, the statistical error bars of the average values in Zhao et al. (2015) are so big that it could also conclude that the decay rate of R_{HVF} does not depend on $\Delta m_{15}(B)$ and $V_{\text{max}}^{\text{Si}}$, which is consistent with my result here.

To confirm above conclusion, I still need to justify that \dot{R}_{HVF} is independent in R_{HVF} . We present the plot of R_{HVF} versus the decay rate of R_{HVF} for CaII IR3 absorption line around maximum brightness in Fig. 17. The figure shows that there is not any potentially correlation between \dot{R}_{HVF} and R_{HVF} , as I expected. In addition, I do not find any potential correlation between \dot{R}_{HVF} of CaII IR3 absorption line and the REW of SiII 635.5 nm absorption line around maximum brightness, either. For simplicity, I do not show the plot again here. So there is indeed a correlation between the strength of CaII IR3 HVF around maximum light in SNe Ia and their stellar population.

In Figs. 16 and 17, I notice that some SNe Ia have a maximum-light \dot{R}_{HVF} value larger than 0, i.e. the strength of CaII IR3 HVF becomes stronger after maximum. For example, $R_{\text{HVF}} = 0.62 \pm 0.07$ at $t = -3.9$ day and $R_{\text{HVF}} = 1.17 \pm 0.02$ at $t = 3.0$ day for SN 1999dq, and $R_{\text{HVF}} = 0.39 \pm 0.05$ at $t = -4.5$ day and $R_{\text{HVF}} = 0.87 \pm 0.10$ at $t = 2.3$ day for SN 2006bt (see table A4 in Silverman et al. 2015). In general, the HVFs appear strongest in early-time spectra and become weak with time, but some well observed SNe Ia show interesting HVF evolutions. As one of the best observed SNe Ia, i.e. SN 2011fe, the strength of the CaII IR3 HVF statistically significantly increases with time during the first week after supernova explosion, and then decreases with time after it reaches to a maximum value (Childress et al. 2014). The evolution of the R_{HVF} of the CaII

IR3 line in SN 2006X also shows a similar behavior to SN 2011fe (see Table A4 in Silverman et al. 2015). In addition, some SNe Ia show a plateau in the evolution curve of R_{HVF} , e.g. SN 2004dt, SN 2009ig and SN 2012fr (Childress et al. 2014; Zhao et al. 2015), Especially, SN 2005cf presents both above behaviors (Zhao et al. 2015). These behaviors on the evolution of the strength of CaII IR3 HVF provide another constraint on the origin of HVFs.

4. DISCUSSION

4.1. Origins of the HVFs

In this paper, based on the published data of CaII IR3 HVF around maximum light in literatures, I found that the SNe Ia with strong CaII IR3 HVF tend to occur in later type host galaxies or early type galaxies with significant recent star formation, and some statistical analysis also show these SNe Ia correlates with relatively younger stellar population than those with weak CaII IR3 HVF. So, my discoveries provide very strong constraints on the origins of HVFs, even on the progenitor and explosion models of SNe Ia. Generally, there are three popular scenarios to explain the origins of the HVFs shown in the spectra of SNe Ia, i.e. the abundance enhancement (AE), density enhancement (DE) and ionization effect (IE) scenarios (Mazzali et al. 2005a; Tanaka et al. 2008; Blondin et al. 2013). Combining with previous results in literatures, I will discuss which scenario is more possible to explain my discoveries in the following sections.

4.1.1. AE scenario

For AE scenario, the outer layers of supernova ejecta are dominated by Si and Ca, which implies that the outer layers of the progenitor WD are significantly burned, or the significant burned materials in inner region are brought up to the outer part of supernova ejecta during the explosion phase (Mazzali et al. 2005a).

Several mechanisms could contribute to above abundance structure. For the delayed-detonation model (Khokhlov 1991), the first deflagration phase may lead to asymmetry for the distribution of detonation ignition point, which could burn C/O into Si/Ca in some directions (Blondin et al. 2013, Seitenzahl et al. 2013). A detonation in

the violent merger of two WDs or a gravitational confined detonation on the surface of WD could also produce a similar situation, i.e. a detonation in one side may produce more high-velocity Si/Ca than the other side (Plewa et al. 2004; Kasen & Plewa 2005; Pakmor et al. 2012). Theoretically, the convection or a high accretion rate before the explosion may naturally lead to an off-center ignition in a WD, and then an asymmetric explosion (Kuhlen et al. 2006; Chen et al. 2014). It has been suggested that the evolution of the photospheric velocity may reflect the fact of an asymmetric explosion, i.e. LVG SNe Ia are observed along the off-center-ignition side, while HVG SNe Ia are observed from another side (Maeda et al. 2010). Polarization observations show that supernova ejecta is not spherically symmetric (Wang & Wheeler 2008). Especially it is found that the higher the REW value of SiII 635.5 nm absorption line, the larger its polarization, which may be explained by the delayed-detonation mode (Meng et al. 2017). However, it is still unclear how the asymmetric explosion affects the HVFs in SNe Ia. In particular, we did not find a difference of the R_{HVF} distribution between LVG SNe Ia and HVG SNe Ia (see Fig. 8), which indicates that the asymmetric explosion could not affect the HVFs in an SN Ia.

If the HVFs in SNe Ia are from above mechanisms, our discoveries indicate that the progenitor population of an SN Ia would affect its explosion, and require that the explosion from a relative young population is more likely to produce Si/Ca at the outer layers of supernova ejecta, and the layers have a higher velocity (see Figs. 6 and 7), or a relatively young population leads to a more asymmetric explosion. At present, it is still unclear how the progenitor population of an SN Ia affect its final explosion, although in principle the initial condition of an exploding CO WD would be determined by its progenitor. Maybe, the cooling time of the initial WD before the onset of accretion or the initial WD mass in a single-degenerate system might play a kind of role (Chen et al. 2014; Meng & Han 2018).

An alternative possibility is from the double-detonation model, in which a He detonation initiated near the WD surface may also produce AE in this region and then show HVFs in the spectra of SNe Ia (Woosley & Kasen 2011; Shen & Moore

2014; Maguire et al. 2014). This mechanism may naturally explain the fact that the line-forming regions for HVF and PVF are detached. The companion of the exploding CO WD may be a helium star or a helium WD. Generally, the systems with helium star companions belong to relative young population, and the systems with helium WDs tend to be old population (Wang et al. 2013; Meng & Han 2015). So, if the abundance enhanced Si/Ca from the double-detonation model is the origin of the HVFs in SNe Ia, our discoveries imply that the systems with helium star companions would produce the more energetic SNe Ia with strong HVFs, while the systems with helium WDs would lead to those with weak HVFs. However, present double-detonation model can not give such a result and no evidence shows that the detonations from helium stars and helium WDs are different. Whatever, this is worth being carefully investigated in the future (Tanikawa et al. 2019).

Another recently explored possibility is that a helium shell flash on a white dwarf with mass close to the Chandrasekhar mass limit could build up a layer enhanced in silicon or calcium pre-SN explosion, where the helium shell is from the accretion of hydrogen or helium from a non-degenerate companion in a single-degenerate system (Kato et al. 2018). The Si/Ca rich material should locate in the most outer layers of supernova ejecta, which would physically separate from the photospheric silicon layers. This might explain the correlation between R_{HVF} and $(\bar{v}_{\text{CI}} - \bar{v}_{\text{Si}})$, but can not explain the SNe Ia with $R_{\text{HVF}} = 0$ and a high value of $(\bar{v}_{\text{CI}} - \bar{v}_{\text{Si}})$. However, it is unclear how this mechanism would relate to the stellar population of SNe Ia. Might there be a difference on the helium flash between young and old populations?

In summary, although the AE scenario may provide a natural way to produce the HVFs, it is completely unclear how this scenario correlates with the stellar population of SNe Ia. In particular, the strength of the HVFs from the AE scenario should decrease with time since the supernova ejecta become thinner and thinner with time, which is quite difficult to explain the increase and plateau behaviors in the R_{HVF} evolution curve with time presented in some well observed SNe Ia, e.g. SN 2011fe, SN 2005cf and SN 2006X (Childress et al. 2014; Zhao et al. 2015; Silverman et al. 2015). So, the origin of the HVFs

in SNe Ia is more possible to be from a mechanism relating to the progenitor models of SNe Ia, rather than explosion models.

4.1.2. DE and IE scenarios

In the DE scenario, the HVFs originate from a high-density or density bump shell (equivalent to adding mass) at outer layers, in which the abundance is a typical value in the expanding ejecta (Mazzali et al. 2005a; Tanaka et al. 2008; Mulligan & Wheeler 2017, 2018). Generally, two mechanisms are suggested to produce the density variation. One is from an asymmetrical explosion, as discussed in the above section. Then, the ejecta in some directions may be affected by burning differently from other directions. As discussed in Sect. 4.1.1, such a mechanism is difficult to explain the correlation between the strength of the maximum-light CaII IR3 HVF and the stellar population of SNe Ia, and is difficult to explain the increase and plateau behavior of the strength evolution of the CaII IR3 HVF shown in some SNe Ia. Another mechanism to achieve density bump shell may be from the interaction between supernova ejecta and relatively dense CSM around progenitor system (Mulligan & Wheeler 2017, 2018).

In the IE scenario, a little amount of hydrogen is mixed at the outermost layer as a source of free electrons. Because Ca is mostly doubly ionized at the outermost layer, the increased free electron density suppress the ionization status of Ca by recombination, and then the fraction of CaII is increased (Mazzali et al. 2005a; Tanaka et al. 2008). The hydrogen may be from a contamination of hydrogen on the WD surface in a single-degenerate system, or from the interaction between supernova ejecta and relatively dense CSM as in DE scenario.

Both DE and IE scenarios have a potential ability, or play a role together, to explain the correlation between the strength of HVFs and the stellar populations of SNe Ia, if the HVFs are from the interaction between the supernova ejecta and the CSM. The interaction between supernova ejecta and the CSM may contribute to the CaII IR3 HVF by the following three ways: I) adding mass at the highest velocity region of supernova ejecta by the accumulation of CSM; II) changing the ionization degree of calcium by increasing the free electron density from hydrogen; III) increasing the residence time of photons in the hydro-

gen shell by a higher scattering-off probability of photons from a higher electron density. All these effects contribute to an increased line absorption at the highest-velocity region of supernova ejecta, and then a HVF is presented in the absorption line of CaII IR3 line in the early optical spectrum of an SN Ia. Because the CaII line is the most remarkable feature in the optical spectrum of an SN Ia, it is also most significantly affected by the interaction between supernova ejecta and the CSM (Mazzali et al. 2005a; Tanaka et al. 2008). Generally, the young SNe Ia tend to have a dense CSM, while the environments around old SNe Ia are relatively clear, e.g. 1991T-like SNe Ia just belong to relatively young population, while no CSM is discovered around old 1991bg-like SNe Ia (Johansson et al. 2013b; Fisher & Jumper 2015). Especially, these two scenarios have a potential ability to explain the evolution of the strength of the HVFs with time. Here, the dominant factor is the decreasing density of supernova ejecta with time, which leads to the global decrease of the strength of the HVFs with time. However, the CSM structure around SNe Ia may be various, depending on the mass-loss histories of their progenitors, e.g. a wind or a shell structure as some SNe Ia shown (Patat et al. 2007; Dilday et al. 2012), which could result in different evolution behaviors of the strength of the HVFs.

Whatever, two special kinds of SNe Ia must be paid more attention, if the HVFs are from the interaction between the supernova ejecta and the hydrogen-rich material, e.g. 2002cx-like and SN Ia-CSM objects (Foley et al. 2013; Silverman et al. 2013). Both kinds of objects belong to relatively young population and have a much denser CSM than normal SNe Ia (Chomiuk et al. 2016; Lyman et al. 2018; Szalai et al. 2019). Meng & Podsiadlowski (2018) even suggested that these two peculiar subclasses of SNe Ia share the same origin, i.e. from the hybrid CONe WD + MS system, based on a new developed version of single-degenerate model [common-envelope wind (CEW) model, Meng & Podsiadlowski 2017]. However, the CaII IR3 absorption features in the spectra of these peculiar SNe Ia are quite different from the normal SNe Ia. For SNe Ia-CSM, the CaII IR3 features are strong and broad emission features, rather than absorption lines in normal SNe Ia (Silverman et al. 2013). Such difference be-

tween SNe Ia-CSM and the normal SNe Ia could arise from the amount of hydrogen-rich material. To form the HVFs in normal SNe Ia, a few $10^{-3} M_{\odot}$ hydrogen-rich materials are enough, but the amount of the CSM around SNe Ia-CSM is much more massive than this value. For example, the amount of the CSM around SN 2002ic (the prototype of SNe Ia-CSM, Hamuy et al. 2003) may be as massive as 0.5-6 M_{\odot} (Chugai & Yungelson 2004; Wang et al. 2004; Kotak et al. 2004). For 2002cx-like SNe Ia, no significant HVF is discovered, but a significantly lower maximum-light expansion velocity than normal SNe Ia becomes a typical character (Foley et al. 2013). The low expansion velocity could result in an overlap or mix line-forming region between the HVFs and PVFs, as shown in some normal SNe Ia with high pEW of photospheric component, but without the high-velocity CaII IR3 lines (see the discussions in Sect.3.3). However, no definitive evidence supports or denies above ideas at present, although SN 2006X provides a clue for the ideas (see Sect.3.3). Especially, it is still unclear how a large amount of hydrogen-rich amount affect the CaII IR3 lines. Then, more efforts on these subjects are needed in the future.

If the HVFs in SNe Ia arise from the interaction between supernova ejecta and hydrogen-rich CSM and the CSM is massive enough, the SNe Ia with very strong HVFs would show a variable sodium absorption lines in their early spectra, as SN 2006X showed (Patat et al. 2007; Simon et al. 2009; Blondin et al. 2009; Ferretti et al. 2016). Recently, Wang et al. (2019) provided a sample of SNe Ia with variable sodium absorption line, including SN 2006X, and these SNe Ia indeed present a strong CaII IR3 HVF. For example, SN 2006X, the prototype of SNe Ia with a variable sodium line, has a maximum-light value of $R_{\text{HVF}} = 1.14 \pm 0.07$ [also for SN 1999dq, 2002bo and 2002cd, see Table A4 in Silverman et al. (2015) and Table 2 in Wang et al. (2019)]. In addition, SN 2002dj presents a quickly variable sodium line around 8 days before maximum light (Fig. 2 in Wang et al. 2019). Interestingly, SN 2002dj also shows a very strong CaII IR3 HVF at the same epoch, i.e. $R_{\text{HVF}} = 1.17 \pm 0.06$ (Table A4 in Silverman et al. 2015). The CSM around SNe Ia may present themselves by another way, i.e. the CSM may redden the color of SNe Ia and

then lead to a color excess, e.g. $E(B - V)$ ⁵. Recently, Bulla et al. (2018) found that some SNe Ia show time-variable $E(B - V)$ and these SNe Ia prefer the SNe Ia with a variable sodium line, e.g. SN 2002bo, 2002cd and 2006X, which also show a very strong maximum-light CaII IR3 HVF. Another interesting fact is that the distribution of the R_{HVF} of the maximum-light CaII IR3 HVF is quite similar to the distribution of the $E(B - V)$ of SNe Ia around maximum brightness, i.e. a low value peak of $R_{\text{HVF}} [E(B - V)]$ with a long tail (Reindl 2005; Meng et al. 2009).

4.2. Progenitor of SNe Ia

The correlation between the strength of the maximum-light CaII IR3 HVF and the stellar population of SNe Ia may provide meaningful constraints on the progenitor models of SNe Ia. In particular, combined with the results in literatures, our discoveries seems to favor that the HVFs in SNe Ia arise from the interaction between supernova ejecta and the CSM around SNe Ia. This is also helpful to distinguish between different progenitor models of SNe Ia. Generally, the progenitors of SNe Ia are categorized into three main scenarios based on the companion nature of the exploding CO WDs and on the explosion mechanism, i.e. the single-degenerate (SD, Whelan & Iben 1973; Nomoto, Thielemann & Yokoi 1984), double-degenerate (DD, Iben & Tutukov 1984; Webbink 1984), and sub-Chandrasekhar double-detonation (D-DET) models (Woosley & Weaver 1994; Livne & Arnett 1995; Shen et al. 2013). In the following sections, I will discuss which model is more likely to explain all the observations of the HVFs in SNe Ia.

4.2.1. SD model

In the SD model, the companion of the exploding CO WD may be a main sequence (MS), a subgiant (SG), a red-giant (RG) or a helium star. The accreted hydrogen-rich or helium-rich material is burned on the surface of the CO WD into carbon and oxygen, and then deposited onto the WD. When the WD mass reaches to a value

⁵The CSM leading to the HVFs in SNe Ia is relatively close to the exploding WD, while the CSM that is far away from the exploding WD may also contribute to the color excess of SNe Ia.

close to the Chandrasekhar mass limit, an SN Ia may be produced. After the supernova explosion, the companion may survive (Wang & Han 2012; Maoz, Mannucci & Nelemans 2014; Meng et al. 2015). If the correlation between the strength of the HVFs and the stellar population arises from the interaction between supernova ejecta and the hydrogen-rich CSM, the SD model has a potential ability to explain the origin of the HVFs, where the CSM is from the outflow or wind from the binary system. For a given initial WD, the amount and density of the CSM is then mainly determined by the initial companion mass, i.e. the more massive the companion, the more likely to form a dense CSM by a wind (e.g. the common-envelope wind, Meng & Podsiadlowski 2017). In addition, the age of an SN Ia from the SD channel is also dominated by the companion mass, i.e. the more massive the companion, the younger the SN Ia. So, a relatively younger SN Ia means a relatively denser CSM, and then a stronger HVFs, i.e. in principle, the SD model may explain my discoveries in this paper. Since the CSM structure may be various depending on the detailed mass-loss histories, the SD model may also explain the increase or plateau behaviors in the CaII IR3 R_{HVF} evolution with time in principle. In addition, based on the SD model, in principle, the CSM may exist anywhere from the vicinity of the progenitor system of an SN Ia to a distance of more than 300 pc to the system, depending on the detailed way that the CSM is formed (Meng & Podsiadlowski 2017, 2018), as deduced from observations (Broersen et al. 2014; Bulla et al. 2018).

A symbiotic system with a low-mass RG could also be the progenitor of an SN Ia (Li & van den Heuvel 1997; Hachisu et al. 1999; Chen et al. 2011). Such a system belongs to an old population, but may also have a relatively dense CSM, which seems to be inconsistent with our discovery. Maybe, a spin-up/spin-down mechanism is necessary (Justham 2011; Di Stefano & Kilic 2012). For this mechanism, the CO WD will not explode as an SN Ia immediately for a rapid rotation, spined up by the accretion, even if its mass reaches to or exceeds the Chandrasekhar mass limit. The rapid rotating WD must experience a spin-down phase to explode, although the spin-down timescale is quite uncertain (Di Stefano et al.

2011; Meng & Podsiadlowski 2013). During the spin-down phase, the environment around the progenitor system may become very clean and the RG companion may become a dim helium WD or sdB star (Justham 2011; Meng & Li 2019). Maybe, the initial WD mass could play a key role for the spin-down timescale (Meng & Han 2018). If so, the SD model is not inconsistent with our discoveries.

The interacting CSM may emit at radio band and X-ray, but no any SN Ia has been detected in radio or in X-ray bands, even for the two most well observed SNe Ia, e.g. SN 2011fe and SN 2014J (Margutti et al. 2012, 2014; Chomiuk et al. 2012; Pérez-Torres et al. 2014). These negative results indicate a very low CSM density around the exploding SNe Ia, which is consistent with the required amount of the hydrogen-rich CSM to explain the HVF of SNe Ia, but without hydrogen emission lines in the spectra of SNe Ia (e.g. a few times of $10^{-3} M_{\odot}$, Mazzali et al. 2005a; Tanaka et al. 2008). Whatever, if the amount of hydrogen-rich CSM is massive enough, the hydrogen emission line would be expected, as shown in the spectra of SNe Ia-CSM (Hamuy et al. 2003; Dilday et al. 2012; Silverman et al. 2013).

4.2.2. DD model

In the DD model, a binary system consisting of two CO WDs loses its orbital angular momentum by gravitational radiation, and merges finally. If the total mass of the binary system exceeds the Chandrasekhar mass limit, the merger may explode as an SN Ia. Whatever, the merger will be disrupted completely and no surviving companion exists after supernova explosion (Wang & Han 2012; Maoz, Mannucci & Nelemans 2014; Meng et al. 2015).

Actually, the CSM may also be formed from a DD system, but it is hydrogen- and helium-deficient, i.e. it mainly consists of carbon/oxygen, where the CSM could arise from a super wind during the merging process (Soker 2013). For example, although they are very rare, the so-called ‘super-Chandrasekhar’ SNe Ia are suggested to be that a Chandrasekhar-mass WD explodes inside a dense carbon/oxygen envelope which is the leftover of the WD-WD merger (Howell et al. 2006; Scalzo et al. 2014; Taubenberger et al. 2013, 2019). If such a kind of CSM plays a role to form

the HVFs in SNe Ia, the origin of HVFs would be the DE scenario.

It was suggested that the younger, more massive stars produce more massive white dwarfs, and then more massive carbon/oxygen envelope to be formed during the merging process (Howell 2011; Maoz & Mannucci 2012), which could contribute to the correlation between the HVFs of SNe Ia and their stellar population. However, the detailed binary population synthesis shows that the distribution of the total masses of the DD systems is rather uniform within the whole delay-time interval because the delay time of SNe Ia from the DD systems is mainly determined by gravitational wave radiation, rather than their progenitor evolutionary time (Meng & Yang 2012), which indicates that the leftover of the WD-WD merger would be the same, whatever the progenitors of SNe Ia belongs to young or old stellar population. Maybe, as needed in the SD model, a spin-down timescale and a magnetic field would be necessary, i.e. for young SNe Ia, the magnetic field of the merger is stronger, and then the spin-down timescale is shorter to form a relatively denser carbon/oxygen CSM (Ilkov & Soker 2012). However, it is completely unclear why younger DD systems would form a merger with stronger magnetic field and then experience a shorter spin-down timescale.

The leftover of the WD-WD merger could have other geometric structure, e.g. the disk-originated CSM, depending on the merger timescale (Levanon et al. 2015; Levanon & Soker 2019). The less massive WD is tidally destroyed by its more massive companion and form an accretion disk around the more massive companion. A bipolar wind or jet might be blown off to form the disk-originated CSM, which is also hydrogen- and helium-deficient. If the interaction between supernova ejecta and the disk-originated CSM is the reason leading to the HVFs in SNe Ia, the DE scenario would be the origin of the HVFs. However, similar to above discussions, many efforts are needed to explore why young SNe Ia have such disk-originated CSM, while old SNe Ia do not, although the distribution of the total mass of the DD systems leading to SNe Ia is rather uniform across the whole delay-time interval (Meng & Yang 2012).

Maybe, both the SD and DD models could produce SNe Ia together, but with different age pop-

ulation, e.g. the SD model mainly produces relatively young SNe Ia and the DD model mainly produces old SNe Ia, since some evidence showed that different SNe Ia may be from different population (Wang et al. 2013). For such a combination of different progenitor models, the IE scenario would be the origin of the HVFs in SNe Ia to explain the correlation between the strength of HVFs and the stellar population of SNe Ia. However, the combination scenario is difficult to explain why almost all SNe Ia show the HVF in very early phase, if the IE scenario is the origin of the HVFs.

As a special case of DD model, the core-degenerate (CD) model may also have an ability to explain the correlation between the maximum-light CaII IR3 HVF and the stellar population of SNe Ia, where the hydrogen-rich CSM is from the common envelope formed by merger between a CO WD and an AGB star with an CO core. (Kashi & Soker 2011). Whatever, similar to the SD model, a spin-down timescale is also necessary to explain the correlation found in this paper, where a magneto-dipole radiation torque dominates the spin-down timescale (Ilkov & Soker 2012). However, it is completely unclear why young merger tends to have a strong magnetic field, and then lead to a short spin-down timescale (Ilkov & Soker 2012). In addition, the CD model is less possible to contribute to the majority of SNe Ia (Meng & Yang 2012; Wang et al. 2017), although the argument on the contribution exists (Ilkov & Soker 2013).

4.2.3. D-DET model

The D-DET model is also frequently discussed, in which the companion of the CO WD is a helium WD or a helium star. The companion fills its Roche lobe and a stable mass transfer occurs. If the mass-transfer rate is not high enough so that the helium-rich material can not be stably burning, the helium will gradually accumulate on the CO WD. When the helium layer is thick enough, a detonation will be ignited at the bottom of the helium shell, where the inward supersonic detonation wave may lead to the second detonation in the center of the CO WD. After the supernova explosion, a hypervelocity companion may survive (Geier et al. 2015; Shen et al. 2018).

The D-DET model could contribute to the HVFs by three different ways. I) there is a

thin hydrogen-rich layer on a helium WD, which will transfer onto the WD prior to the He core's tidal disruption. Finally, this hydrogen-rich material will be ejected from the binary system via a way similar to a classical nova to form the CSM (Shen et al. 2013). The interaction between supernova ejecta and the CSM could contribute to the HVFs in SNe Ia. A key problem for this scenario is whether the amount of the CSM is enough or not, since the hydrogen-rich layer on a He WD is generally only $2 \times 10^{-4} - 2 \times 10^{-3} M_{\odot}$ and a part of hydrogen-rich material will be consumed during classical nova explosion phase, while $4 - 5 \times 10^{-3} M_{\odot}$ hydrogen rich material is necessary for IE scenario (Shen et al. 2013; Mazzali et al. 2005a; Tanaka et al. 2008). Maybe, both DE and IE scenarios play a role together to form the HVFs in SNe Ia here. II) as discussed in Sect. 4.1.1, the first detonation may directly produce high-velocity Si/Ca in the outer layer of supernova ejecta (Shen & Moore 2014). III) a dense helium shell may exist prior to the complete explosion of the white dwarf, which is ejected by the detonation on the surface of the white dwarf or arises from the accretion on to the progenitor white dwarf (Shen et al. 2010; Shen & Moore 2014). The HVFs, especially the CaII IR3 feature, may be explained by the interaction between supernova ejecta and the dense helium shell (Mulligan & Wheeler 2017, 2018). Whatever the way is, it is unclear why young SNe Ia produce strong HVFs, while old SNe Ia produce weak HVFs for the D-DET model. The D-DET model is also relatively difficult to explain the various evolution behaviors of the R_{HVF} of CaII IR3 absorption line with time.

4.3. Origin of the relation between R_{HVF} and $(\bar{v}_{\text{CI}} - \bar{v}_{\text{Si}})$

In section 3.3, I found that there is very good linear relation between R_{HVF} and $(\bar{v}_{\text{CI}} - \bar{v}_{\text{Si}})$, and suggest $(\bar{v}_{\text{CI}} - \bar{v}_{\text{Si}})$ as an indicator to judge whether or not there is a high-velocity component in CaII IR3 absorption line. This relation could provide important clues on explosion mechanism of SNe Ia and the origin of the HVFs in SNe Ia.

From Figs. 6 and 7, CaII IR3 line usually has a larger absorption-weighted velocity than SiII 635.5 nm line. Considering that different elements locate different layers in supernova ejecta

(Filippenko 1997, Mazzali et al. 2007), these results indicate that calcium layer has a higher average velocity than silicon layer. As discussed in above sections, some mechanisms, e.g. asymmetric explosion and double detonation, could contribute to the results, but seem to be difficult to explain the correlation between the strength of CaII IR3 HVF and the population of SNe Ia. In other words, these mechanisms have more or less difficulties to simultaneously explain why R_{HVF} linearly increases with $(\bar{v}_{\text{CI}} - \bar{v}_{\text{Si}})$ and why R_{HVF} depends on the stellar population of SNe Ia.

However, there might be a very simple explanation on the relation in Fig. 6, i.e. the silicon and calcium layers have a similar velocity distribution in the velocity space of supernova ejecta, but the IE is the origin of CaII IR3 HVF. Because calcium has much lower number density than silicon in the forming region of HVF and the calcium ion is more likely to be affected by free electron from hydrogen than silicon, a small amount of hydrogen could lead to a more significant HVF in CaII IR3 line than in SiII 635.5 nm line, i.e. the weighted mean absorption velocity of CaII IR3 line becomes larger than that of SiII 635.5 nm line (see the discussion in Mazzali et al. 2005a). At the same time, the strength of CaII IR3 HVF becomes larger. This simple explanation is also relatively easy to explain why CaII IR3 absorption line usually shows more significant HVF than SiII 635.5 nm line. Whatever, more detailed efforts are needed to verify such an idea.

5. CONCLUSIONS

Although many data on the HVFs of SNe Ia have been published, the origin of the HVFs is still unclear. Especially, no definitive constraint on the progenitor or explosion model was obtained from the HVF observation. In this paper, based on the data published in literatures, I found strong evidence that the strength of the CaII IR3 HVF around maximum brightness correlates with the stellar population of SNe Ia, and the main results are as follows.

1) SNe Ia with strong CaII IR3 HVF around maximum brightness tend to occur in late-type galaxies. Some lenticular galaxies also host the SNe Ia with strong CaII IR3 HVF, but all of these lenticular galaxies show the signature of recent

or on-going star formation, and the SNe Ia with strong maximum-light CaII IR3 HVF locate at or close to the star formation regions in their host galaxies.

2) In the sample of Silverman et al. (2015), all of the eight 1991T-like SNe Ia have a very strong CaII IR3 HVF around maximum light, while among seventeen 1991bg-like SNe Ia, sixteen present weak or no CaII IR3 HVF around maximum brightness. It is well established that 1991T-like SNe Ia arise from young stellar population and 1991bg-like SNe Ia belong to old stellar population

3) By pixel statistics, I found that the SNe Ia with strong CaII IR3 HVF around maximum brightness show a higher degree of association with star formation index, e.g. $H\alpha$ or near-UV emission, than those with weak maximum-light CaII IR3 HVF.

4) Because all the host galaxies are star-forming galaxies in the sample of Anderson et al. (2015b), the sample size of SNe Ia with weak maximum-light CaII IR3 HVF is much smaller than that with strong maximum-light CaII IR3 HVF (see Sect. 3.8).

5) The distribution of the REW of SiII 635.5 nm around maximum brightness between the SNe Ia with strong and weak CaII IR3 HVF are quite different, i.e. SNe Ia with strong maximum-light CaII IR3 HVF favor small or larger REW, while those with weak maximum-light CaII IR3 HVF tend to have a middle value of REW.

6) I found that the strength of the CaII IR3 HVF around maximum brightness is linearly dependent on the difference of the absorption-weighted velocities between CaII IR3 and SiII 635.5 nm absorption lines at the same phase. Then, I suggest that the difference of the absorption-weighted velocities may be helpful to judge whether or not there is a high-velocity component in the CaII IR3 feature in the spectra of SNe Ia.

Based on the above results, I may get a conclusion that the SNe Ia with strong CaII IR3 HVF around maximum brightness favor relatively younger stellar population than those with weak maximum-light CaII IR3 HVF, which provides meaningful constraints on the explosion and progenitor models. Although a spin-up/spin-down

mechanism is necessary, the SD model may relatively naturally explain the correlation between the strength of the HVFs and the stellar population of SNe Ia discovered here, while more efforts for the DD and D-DET models are necessary. Although our results can not give a definitive conclusion on the origin of the HVFs, the discoveries here seem to disfavor the AE scenario as the origin of the HVFs, and the HVFs are less possible to arise from the explosion itself of an SN Ia. On the contrary, the interaction between supernova ejecta and the hydrogen-rich CSM could be a natural origin of the HVFs in SNe Ia, where the DE and IE scenarios could play a role together.

Acknowledgments

I am grateful to the anonymous referee for his/her constructive comments which help me to improve the manuscript. I thank Zhengwei Liu, Callum McCutcheon and Philipp Podsiadlowski for their helpful discussions. This work was partly supported by the NSFC (Nos. 11973080 and 11733008), Yunnan Foundation (No. 2015HB096 and 2017HC018), and CAS (No. KJZD-EW-M06-01). X.M. thanks the support by Yunnan Ten Thousand Talents Plan - Young & Elite Talents Project.

REFERENCES

Abbott, T.M.C., Allam, S., Andersen, P. et al., 2019, *ApJL*, 872, L30

Anderson, J.P. & James, P.A., 2008, *MNRAS*, 390, 1527

Anderson, J. P., James, P. A., Habergham, S. M., Galbany, L., Kuncarayakti, H., 2015a, *PASA*, 32, 19

Anderson, J. P. James, P. A. Förster, F. et al., 2015b, *MNRAS*, 448, 732

Ann, H.B., Seo, M., Ha, D.K, 2015, *ApJS*, 217, 27

Balzano, V.A., 1983, *ApJ*, 268, 602

Benetti, S., Cappellaro, E., Mazzali, P. A. et al., 2005, *ApJ*, 623, 1011

Blondin, S., Prieto, J.L., Patat, F. et al., 2009, *ApJ*, 693, 207

Blondin S., Dessart L., Hillier D. J., Khokhlov A. M., 2013, *MNRAS*, 429, 2127

Bulla, M., Goobar, A., Dhawan, S., 2018, *MNRAS*, 479, 3663

Branch, D., Dang, L. C., & Baron, E. 2009, *PASP*, 121, 238

Broersen, S., Chiotellis, A., Vink, J., Bamba, A., 2014, *MNRAS*, 441, 3040

Cameron, E., 2011, *PASA*, 28, 128

Chugai, N.N., Yungelson L.R., 2004, *Astronomy Letters*, 30, 65

Chen X., Han, Z., Tout, C. A., 2011, *ApJL*, 735, L31

Chen X., Han, Z., Meng, X., 2014, *MNRAS*, 438, 3358

Chevalier, R. A., 1990, in *Supernovae*, ed. A. G. Petschek (New York: Springer-Verlag), 91

Childress M. J., Filippenko A. V., Ganeshalingam M., Schmidt B. P., 2014, *MNRAS*, 437, 338

Chomiuk, L., Soderberg, A., Moe, M., et al. 2012, *ApJ*, 750, 164

Chomiuk, L., Soderberg, A. M., Chevalier, R. A., et al. 2016, *ApJ*, 821, 119

Della Valle, M. & Livio, M., 1994, *ApJ*, 423, L31

Dilday B., Howell D.A., Cenko S.B. et al., 2012, *Science*, 337, 942

Di Stefano R., Voss R., & Claeys J.S.W., 2011, *ApJL*, 738, L1

Di Stefano R., & Kilic M. 2012, *ApJ*, 759, 56

Filippenko, A.V., 1997, *ARA&A*, 35, 309

Ferretti, R., Amanullah, R., Goobar, A. et al., 2016, *A&A*, 592, A40

Fisher, R. & Jumper, K., 2015, *ApJ*, 805, 150

Foley, R. J., Challis, P. J., Chornock, R., et al. 2013, *ApJ*, 765, 57

Fruchter, A. S., Levan, A. J., Strolger, L. et al., 2006, *Nature*, 441, 463

- Gall, C., Stritzinger, M. D., Ashall, C. et al., 2018, *A&A*, 611, A58
- Geier, S., Fürst, F., Ziegerer, E. et al., 2015, *Science*, 347, 1126
- Goobar, A. & Leibundgut, B., 2011, *ARNPS*, 61, 251
- Hachisu, I., Kato, M., Nomoto, K., 1999, *ApJ*, 522, 487
- Hamuy M., Phillips M.M., Schommer R.A. et al., 1996, *AJ*, 112, 2391
- Hamuy, M., Phillips, M. M., Suntzeff, N. B. et al., 2003, *Nature*, 424, 651
- Hatano, K., Branch, D., Fisher, A., Baron, E., Filippenko, A.V., 1999, *ApJ*, 525, 881
- Hillebrandt, W., Niemeyer, J.C., 2000, *ARA&A*, 38, 191
- Hillebrandt, W., Kromer, M., Röpke, F. K., Ruiter, A. J., 2013, *FrPhy*, 8, 116
- Howell, D. A. 2001, *ApJ*, 554, L193
- Howell D.A., Sullivan, M., Nugent, P.E. et al., 2006, *Nature*, 443, 308
- Howell, D.A., 2011, *NatCo*, 2E, 350
- Hoyle, F. & Fowler, W.A., 1960, *ApJ*, 132, 565
- Iben, I., Tutukov, A.V., 1984, *ApJS*, 54, 335
- Ilkov, M., Soker, N., 2012, *MNRAS*, 419, 1695
- Ilkov, M., Soker, N., 2013, *MNRAS*, 428, 579
- Jha, S.W., Maguire, K. & Sullivan, M., 2019, *NatAs*, 3, 706
- Johansson, J., Thomas, D., Pforr, J. et al., 2013a, *MNRAS*, 435, 1680
- Johansson, J., Amanullah, R., Goobar, A., 2013b, *MNRAS*, 431, L43
- Justham S., 2011, *ApJL*, 730, L34
- Kashi, A. & Soker N. 2011, *MNRAS*, 417, 1466
- Kasen D., Nugent, P., Wang, L. et al., 2003, *ApJ*, 593, 788
- Kasen, D., Plewa, T., 2005, *ApJ*, 622, L41
- Kato, M., Saio, H., Hachisu, I., 2018, *ApJ*, 863, 125
- Khokhlov, A.M., 1991, *A&A*, 245, 114
- Kotak, R., Meikle, W.P.S., Adamson, S. et al., 2004, *MNRAS*, 354, L13
- Kuhlen, M., Woosley, S.E. & Glatzmaier, G.A., 2006, *ApJ*, 640, 407
- Levanon, N., Soker, N., & García-Berro, E., 2015, *MNRAS*, 447, 2803
- Levanon, N., Soker, N., 2019, *ApJL*, 872, L7
- Li, X.D., van den Heuvel, E.P.J., 1997, *A&A*, 322, L9
- Li, W.-D., Bloom, J. S., Podsiadlowski, Ph. et al., 2011, *Nature*, 480, 348
- Livne, E., & Arnett, D., 1995, *ApJ*, 452, 62
- Lyman, J. D., Taddia, F., Stritzinger, M. D., et al. 2018, *MNRAS*, 473, 1359
- Mannucci, F., Della Valle, M., Panagia, N. et al., 2005, *A&A*, 433, 807
- Maoz, D., & Mannucci, F., 2012, *PASA*, 29, 447
- Maoz D., Mannucci F., Nelemans G., 2014, *ARA&A*, 52, 107
- Maeda, K., Benetti, S., Stritzinger, M. et al., 2010, *Nature*, 466, 82
- Maguire K., Sullivan, M., Ellis, R.S. et al., 2012, *MNRAS*, 426, 2359
- Maguire K., Sullivan, M., Pan, Y.-C. et al., 2014, *MNRAS*, 444, 3258
- Maguire, K., Sim, S.A., Shingles, L. et al., 2018, *MNRAS*, 477, 3567
- Margutti, R., Soderberg, A. M., Chomiuk, L., et al. 2012, *ApJ*, 751, 134
- Margutti, R., Parrent, J., Kamble, A., et al. 2014, *ApJ*, 790, 52
- Marino, A., Rampazzo, R., Bianchi, L. et al., 2011, *MNRAS*, 411, 311

- Marion, G. H., Vinko, J., Wheeler, J. C. et al., 2013, *ApJ*, 777, 40
- Maund, J. R., Spyromilio, J., Höflich, P. A. et al., 2013, *MNRAS*, 433, L20
- Mazzali P.A., Benetti S., Stehle M. et al., 2005a, *MNRAS*, 357, 200
- Mazzali P.A., Benetti S., Altavilla G. et al., 2005b, *ApJL*, 623, L37
- Mazzali, P.A., Röpke, F.K., Benetti, S., Hillebrandt, W., 2007, *Science*, 315, 825
- McCully, C., Jha, S. W., Foley, R. J. et al., 2014, *Nature*, 512, 54
- Meng, X., Chen, X., Han, Z., Yang, W., 2009, *RA&A*, 9, 1259,
- Meng X., & Yang W., 2012, *A&A*, 543, A137
- Meng, X. & Podsiadlowski, Ph., 2013, *ApJL*, 778, L35
- Meng X., Gao Y., Han Z., 2015, *IJMPD*, 24, 14, 1530029
- Meng, X., Han, Z., 2015, *A&A*, 573, A57
- Meng, X. & Podsiadlowski, Ph., 2017, *MNRAS*, 469, 4763
- Meng, X., Zhang, J., Han, Z., 2017, *ApJ*, 841, 62
- Meng, X., Han, Z., 2018, *ApJL*, 855, L18
- Meng, X. & Podsiadlowski, Ph., 2018, *ApJ*, 861, 127
- Meng, X. & Li, J., 2019, *MNRAS*, 482, 5651
- Mulligan, B.W., Wheeler, J.C., 2017, *MNRAS*, 467, 778
- Mulligan, B.W., Wheeler, J.C., 2018, *MNRAS*, 476, 1299
- Navasardyan, H., Petrosian, A.R., Turatto, M., Cappellaro, E., Boulesteix, J., 2001, *MNRAS*, 328, 1181
- Nomoto, K., Thielemann, F-K., Yokoi, K., 1984, *ApJ*, 286, 644
- Pakmor, R., Kromer, M., Taubenberger, S. et al., 2012, *ApJ*, 747, L10
- Pan, Y.-C., Sullivan, M., Maguire, K. et al., 2015, *MNRAS*, 446, 354
- Parrent J., Howell, D. A., Friesen, B. et al., 2012, *ApJ*, 752, L26
- Pastorello, A., Taubenberger, S., Elias-Rosa, N. et al., 2007, *MN*, 376, 1301
- Patat, E., Chandra, P., Chevalier, R., et al., 2007, *Science*, 317, 924
- Patat F., Baade D., Höflich P. et al. 2009, *A&A*, 508, 229
- Pérez-Torres, M., Lundqvist, P., Beswick, R., et al. 2014, *ApJ*, 792, 38
- Planck Collaboration, Aghanim, N., Akrami, Y., et al. 2018, *arXiv:1807.06209*
- Plewa, T., Calder, A. C., & Lamb, D. Q. 2004, *ApJL*, 612, L37
- Perlmutter, S., Gabi, S., Goldhaber, G., et al., 1997, *ApJ*, 483, 565
- Perlmutter, S., Aldering, G., Goldhaber, G. et al., 1999, *ApJ*, 517, 565
- Phillips M.M., 1993, *ApJ*, 413, L105
- Reindl, B., Tammann, G. A., Sandage, A. et al. 2005, *ApJ*, 624, 532
- Riess, A., Press, W. H., Kirshner, R. P., 1996, *ApJ*, 473, 88
- Riess, A., Filippenko, A. V., Challis, P., et al., 1998, *AJ*, 116, 1009
- Riess A.G., Macri L.M., Hoffmann S.L. et al., 2016, *ApJ*, 826, 56
- Salim, S., Charlot, S., Rich, R.M. et al., 2005, *ApJ*, 619, L39
- Scalzo, R. A., Ruiter, A. J., Sim, S. A., 2014, *MNRAS*, 445, 2535
- Schawinski, K., Kaviraj, S., Khochfar, S. et al., 2007, *ApJS*, 173, 512
- Seitzzahl, I.R., Ciaraldi-Schoolmann, F., Röpke, F.K. et al. 2013, *MNRAS*, 429, 1156
- Shen, K.J., Kasen, D., Weinberg, N.N., Bildsten, L., Scannapieco, E., 2010, *ApJ*, 715, 767

- Shen, K.J., Guillochon, J., Foley, R.J., 2013, *ApJ*, 770, L35.
- Shen, K.J., Moore, K., 2014, *ApJ*, 797, 46
- Shen, K.J., Boubert, D.m, Gänsicke, B.T. et al., 2018, *ApJ*, 865, 15
- Sheardown, A., Roediger, E., Su, Y. et al., 2018, *ApJ*, 865, 118
- Silverman, J. M., Kong, J. J., & Filippenko, A. V. 2012a, *MNRAS*, 425, 1819
- Silverman, J. M., Foley, R J., Filippenko, A.V. et al., 2012b, *MNRAS*, 425, 1789
- Silverman, J. M., Nugent, P. E., Gal-Yam, A. et al., 2013, *ApJS*, 207, 3
- Silverman, J. M.; Vinkó, J., Marion, G.H. et al., 2015, *MNRAS*, 451, 1973
- Simon, J.D., Gal-Yam, A., Gnat, O., et al., 2009. *ApJ* 702, 1157
- Smith, B.J., Giroux, M.L., Struck, C., Hancock, M., 2010, *AJ*, 139, 1212
- Soker, N., 2013, *IAUS*, 281, 72
- Sternberg, A., Gal-Yam, A., Simon, J. D. et al., 2011, *Science*, 333, 856
- Su, Y., Kraft, R.P., Roediger, E. et al., 2017, *ApJ*, 834, 74
- Sullivan, M., Le Borgne, D., & Pritchett, C. J., et al. 2006, *ApJ*, 648, 868
- Sullivan, M., Guy, J., Conley, A. et al., 2011, *ApJ*, 737, 102
- Szalai, T., Zsíros, S., Fox, O.D., Pejcha, O., Müller, T., 2019, *ApJS*, 241, 38
- Tanaka M., Mazzali, P.A., Benetti, S. et al., 2008, *ApJ*, 677, 448
- Tanikawa, A., Nomoto, K., Nakasato, N., Maeda, K., 2019, *ApJ*, in press, arXiv: 1909.09770
- Taubenberger, S., Kromer, M., Hachinger, S. et al., 2013, *MNRAS*, 432, 3117
- Taubenberger1, S., Floers1, A., Vogl, C. et al., 2019, in press, arXiv: 1907, 6753
- Véron-Cetty, M.-P. & Véron, P., 2006, *A&A*, 455, 773
- Wang, L., Höflich, P., Wheeler, J.C., 1997, *ApJ*, 483, L29
- Wang, L., Baade, D., Höflich, P. et al., 2003, *ApJ*, 591, 1110
- Wang L., Baade D., Höflich P. et al., 2004, *ApJ*, 604, L53
- Wang L., Baade D., Höflich P. et al. 2006, *ApJ*, 653, 490
- Wang, L., & Wheeler, J. C. 2008, *ARA&A*, 46, 433
- Wang, X., Filippenko, A. V., Ganeshalingam, M. et al., 2009, *ApJ*, 699, L139
- Wang, X., Wang, L., Filippenko, A. V., et al. 2013, *Sci*, 340, 170
- Wang, X., Chen, J., Wang, L. et al., 2019, *ApJ*, in press, arXiv: 1810.11936
- Wang, B., Han, Z., 2012, *NewAR*, 56, 122
- Wang, B., Justham, S., Han, Z., 2013, *A&A*, 559, A94
- Wang, B., Zhou, W.-H., Zuo, Z.-Y. et al., 2017, *MNRAS*, 464, 3965
- Webbink, R.F., 1984, *ApJ*, 277, 355
- Whelan, J., Iben, I., 1973, *ApJ*, 186, 1007
- Woosley, S.E. & Weaver, T.A., 1994, *ApJ*, 423, 371.
- Woosley, S.E., & Kasen, D., 2011, *ApJ*, 734, 38
- Zhang, J., Wang, X., Sasdelli, M. et al., 2016, *ApJ*, 817, 114
- Zhao, X., Wang, X., Maeda, K. et al., 2015, *ApJS*, 220, 20

This 2-column preprint was prepared with the AAS L^AT_EX macros v5.2.

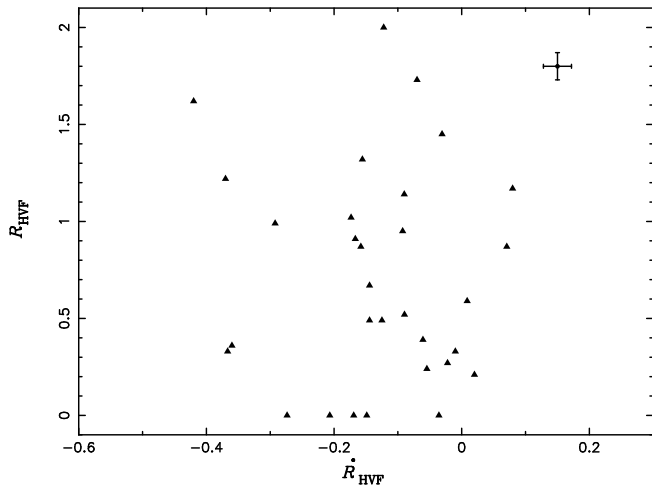


Fig. 17.— R_{HVF} versus the decay rate of R_{HVF} for CaII IR3 absorption line around maximum brightness, where the data are from Silverman et al. (2015). The cross shows the typical error of the data.